PERFORMANCE ANALYSIS OF A DIGITAL COMMUNICATION SYSTEM ON SEA PLATFORMS

A THESIS SUBMITTED TO
THE GRADUATE SCHOOL OF NATURAL AND APPLIED SCIENCES
OF
MIDDLE EAST TECHNICAL UNIVERSITY

BY

GÖKBERK ŞENOL

IN PARTIAL FULLFILLMENT OF THE REQUIREMENTS
FOR
THE DEGREE OF MASTER OF SCIENCE
IN
ELECTRICAL AND ELECTRONICS ENGINEERING

OCTOBER 2012

Approval of the thesis:

PERFORMANCE ANALYSIS OF A DIGITAL COMMUNICATION SYSTEM ON SEA PLATFORMS

submitted by **GÖKBERK ŞENOL** in partial fulfillment of the requirements for the degree of **Master of Science in Electrical and Electronics Engineering Department, Middle East Technical University** by,

Prof. Dr. Canan Özgen _____

Dean, Graduate School of **Natural and Applied Sciences**

Prof. Dr. İsmet Erkmen _____

Head of Department, **Electrical and Electronics Engineering**

Prof. Dr. Yalçın Tanık _____

Supervisor, **Electrical and Electronics Engineering Dept., METU**

Examining Committee Members:

Prof. Dr. Mete Severcan _____

Electrical and Electronics Engineering Dept., METU

Prof. Dr. Yalçın Tanık _____

Electrical and Electronics Engineering Dept., METU

Assist. Prof. Dr. Melek Diker Yücel _____

Electrical and Electronics Engineering Dept., METU

Assist. Prof. Dr. Ali Özgür Yılmaz _____

Electrical and Electronics Engineering Dept., METU

Dr. Alime Özyıldırım _____

ASELSAN, REHİS

Date: **05.10.2012**

I hereby declare that all information in this document has been obtained and presented in accordance with academic rules and ethical conduct. I also declare that, as required by these rules and conduct, I have fully cited and referenced all material and results that are not original to this work.

Name, Last name : GÖKBERK ŞENOL

Signature :

ABSTRACT

PERFORMANCE ANALYSIS OF A DIGITAL COMMUNICATION SYSTEM ON SEA PLATFORMS

Şenol, Gökberk

M. Sc., Department of Electrical and Electronics Engineering
Supervisor: Prof. Dr. Yalçın Tanık

October 2012, 87 pages

The transmission rate and reliability are the most crucial elements of a communication system on sea platforms. In this thesis, the performance of a high speed and reliable communication system that can be used on ship to ship sea platforms will be evaluated.

The two ray channel model is used in order to characterize the channel considering the refraction and reflection. Using the channel model, the path loss and the Shannon channel capacities are obtained for different systems.

In order to increase the system performance, frequency diversity technique is used and a detailed comparison of diversity combining techniques is provided.

As an alternative to Shannon channel capacity, cut off rate analysis is considered to get more realistic results about the rate of the communication system in that it takes modulation into account and the results are compared with the channel capacity. Block fading model and jamming effects on the achievable rate of the system is considered for different linear modulation techniques.

Finally, an OFDM system design is given as an example using the tools obtained in this work.

Keywords: Channel capacity, cutoff rate, frequency diversity, sea platforms

ÖZ

DENİZ PLATFORMLARINDAKİ SAYISAL BİR HABERLEŞME SİSTEMİNİN BAŞARIM ÇÖZÜMLEMESİ

Şenol, Gökberk

Yüksek Lisans, Elektrik Elektronik Mühendisliği Bölümü
Tez Yöneticisi: Prof. Dr. Yalçın Tanık

Ekim 2012, 87 sayfa

İletim hızı ve güvenilirlik deniz platformlarında kullanılan bir haberleşme sisteminin en önemli özellikleridir. Bu tezde, gemi-gemi arasındaki deniz platformlarında kullanılabilecek yüksek hızlı ve güvenilir bir haberleşme sisteminin başarımı incelenmiştir.

Kanalı tanımlamak için, kırılma ve yansıma etkilerini de içeren iki yollu bir kanal modeli kullanılmıştır. Kanal modeli kullanılarak, farklı sistemler için yol kaybı ve Shannon kanal kapasitesi değerleri elde edilmiştir.

Sistem başarımını arttırmak için frekans çeşitleme yöntemi kullanılmış ve alıcıda farklı birleştirme yöntemlerinin detaylı bir karşılaştırması yapılmıştır.

Shannon kanal kapasitesine alternatif olarak, haberleşme sisteminin hızı hakkında daha gerçekçi sonuçlar elde etmek için, kanal kapasitesinde modülasyonun etkisini de içeren kesilme oranı incelenmiş ve sonuçlar kanal kapasitesi ile karşılaştırılmıştır. Farklı doğrusal modülasyon teknikleri için, blok zayıflama modeli ve karıştırmanın, ulaşılabilir hıza etkisi incelenmiştir.

Son olarak, bu tezde anlatılan sistem tasarım ilkeleri kullanılarak bir OFDM sistem örneği verilmiştir.

Anahtar Kelimeler: Kanal kapasitesi, kesilme oranı, frekans çeşitleme, deniz platformları

To My Family

ACKNOWLEDGEMENTS

I would like to express my deepest gratitude to my supervisor Prof. Dr. Yalçın TANIK for his guidance, advice and support throughout this study.

I am also grateful to ASELSAN Inc. for the facilities provided for the completion of this thesis.

I would like to thank to my father, my mother and my brother for their continuous encouragement and support.

TABLE OF CONTENTS

LIST OF TABLES

TABLES

LIST OF FIGURES

FIGURES

LIST OF ABBREVIATIONS

PL	: Path Loss
LOS	: Line of Sight
m	: meter
km	: kilometer
sec	: second
bps	: bits per second
Mbps	: Megabits per second
AWGN	: Additive White Gaussian Noise
rms	: root mean square
SNR	: Signal to Noise Ratio
SS	: Selection Switching
MRC	: Maximal Ratio Combining
EGC	: Equal Gain Combining
QAM	: Quadrature Amplitude Modulation
PAM	: Pulse Amplitude Modulation
FHSS	: Frequency Hopping Spread Spectrum
OFDM	: Orthogonal Frequency Division Multiplexing
FDM	: Frequency Division Multiplexing
CSIT	: Channel State Information at Transmitter

CHAPTER 1

INTRODUCTION

1.1 SCOPE AND OBJECTIVES

In this thesis, our aim is to develop design tools for a high rate and reliable communication system in ship to ship sea platforms. While doing that; a communication channel model, namely the two ray channel model, is used and by changing the various parameters such as distance, frequency and modulation; the channel capacity and the cut off rate of the systems are obtained. Channel capacity improvements for different diversity combining techniques are also compared. In order to make the propagation channel more reliable, jamming effect on system design is considered and results are reported. Finally, by using all this information some system design examples are provided.

A communication system mainly consists of transmitter, receiver and propagation channel as shown in Figure 1-1.

Figure 1-1: Basic communication system components

System designer has a certain control on the receiver and transmitter systems by needs of the communication system. However, channel parameters are mostly dependent on external entities. When a signal passes through a wireless channel, it is subject to several effects such as addition of noise, fading, interference, reflection etc. For this reason, it is necessary to know the characteristics of the channel to design a high rate and reliable communication system.

In different media, the transmitted signal will encounter multiple objects that produce reflected, diffracted or scattered copies of the transmitted signal. Because there are fewer obstacles on sea platforms compared to other media, the two ray channel model is used in order to characterize the channel parameters on sea platforms. The two ray channel model is used when only the reflection from ground plane dominates other multipath components [1, 2]. In two ray channel model, the signal from transmitter to receiver is considered to travel in only two paths: the line of sight path and the reflected path as shown in Figure 1-2.

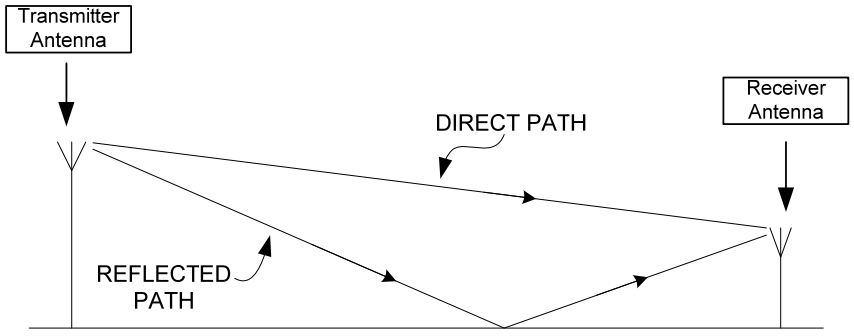

Figure 1-2: The two ray channel model

The reflected signal consists of the specular and diffuse components. When the surface is smooth, the specular component dominates; when the surface is rough both specular and diffuse components are observed. The specular component is coherent part of the reflected signal. In case of rough surface reflection, the energy

of the signal which is not reflected specularly will be scattered from the rough surface at various angles in a random manner. This is known as the diffuse component [15].

Channel capacity is an important measure of a communication system that reveals the ultimate system performance. The distance between the transmitter and receiver antennas, the frequency of the transmitted signal, the transmitted power and the bandwidth of the channel are main parameters that affect the capacity of a channel. In the following chapters, the path loss of the channel and its capacity are evaluated by changing the various design parameters that affect the system performance and results are compared.

Diversity techniques can be used to improve the system performance in fading channels. Instead of transmitting and receiving the desired signal through a single channel, different copies of the signal that are essentially independent may be utilized for increasing the system performance [5]. For example, when the signals are transmitted at frequencies that are separated at least one coherence bandwidth, the signals undergo independent fading.

At the receiver side, the transmitted signal may be processed by several techniques. In this work, the following 3 combining techniques are used:

1. Selection Switching (SS)
2. Equal Gain Combining (EGC)
3. Maximal Ratio Combining (MRC)

In the following chapters of this thesis, different diversity combining techniques are compared.

As an alternative to the channel capacity, the cutoff rate approach is used. The cutoff rate approach is mainly based on randomly selected codes for achievable rate

of any coded modulation system for a given constellation [6].Therefore we also provide a cut off rate analysis.

Frequency hopping may be considered in reliable system designs to combat jamming. Therefore, we use frequency hopping as a method of providing diversity.

Finally, considering all major parameters in a communication system, high rate and reliable system design examples developed and their performances are provided.

1.2 OUTLINE OF THE THESIS

The thesis is organized as follows:

- Chapter 2 describes the properties of the two ray channel model, which is used throughout this thesis.
- Chapter 3 provides the derivation of the path loss and capacity of the channel.
- Chapter 4 describes the diversity combining techniques and provides a comparison of these techniques.
- Chapter 5 is about the development of the cut off rate for our design including the jamming scenario.
- Chapter 6 explains the conclusions drawn from this work.

CHAPTER 2

MULTIPATH CHANNEL MODEL

In a wireless communication system, the channel model plays the most important role. The ultimate performance of a wireless communication channel is mainly determined by the characteristics of the channel [1].

In this chapter, the channel model relevant to our work and the related phenomena, such as reflection and refraction, are reviewed.

2.1 TWO RAY CHANNEL MODEL

In a communication system, the transmitted signal may be subject to several deteriorating effects depending on the characteristics of the channel. Fading, interference, reflection due to obstacles are some examples. Knowledge of the associated properties of these effects is necessary for a successful design of a communication system.

In a typical urban or indoor environment, a radio signal transmitted form a fixed source will encounter multiple objects in the environment that produce reflected, diffracted or scattered copies of the transmitted signal. These additional copies of the transmitted signal, called multipath signal components, can be attenuated in power, delayed in time, and shifted in phase and/or frequency from the LOS path signal path at the receiver. The multipath signals are summed together at the receiver, which often produces distortion in the received signal relative to the transmitted signal [2]. Different than the urban or indoor environments, the signal is

subject to fewer obstacles on sea platforms. Due to that reason, the multipath signal may be considered only as the reflected signal from the sea surface. Although there exists several channel models for different media, the two ray channel model is used in this work in order to characterize the effect of channel on sea platforms. In this model, it is assumed that the ships are almost stationary and the channel is time invariant.

In two ray channel model, the signal reflected from sea surface dominates the other multipath components. So the signal from the transmitter antenna to the receiver antenna can be considered to travel in only two paths:

- *The Direct (Line of Sight) Path,*
- *The Reflected Path.*

The other multipath components, if present, are assumed to be negligible and can be ignored.

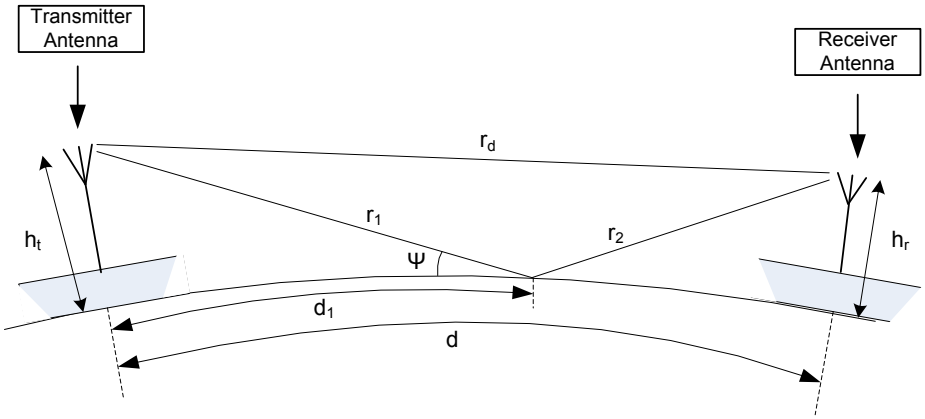

Figure 2-1: The two ray channel geometry

The diagram in Figure 2-1, is used to depict main parameters related to the channel geometry:

h_t : *the transmitter antenna height from the sea surface,*

h_r : *the receiver antenna height from the sea surface,*

r_d : *the direct path distance,*

r_r : *the reflected path distance* $= (r_1 + r_2)$,

d : *the horizontal distance of the transmitter and the receiver antennas,*

d_1 : *the distance from transmitter antenna to the reflection point,*

Ψ : *the grazing angle, the angle between reflected signal and sea surface.*

In two ray channel model, by superposition, the received signal is given as [1, 2]:

$$r(t) = Re\left\{\frac{\lambda}{4\pi}\left[\frac{\sqrt{G_t G_r}\; e^{-j2\pi\frac{r_d}{\lambda}}\, u(t)}{r_d} + R\frac{\sqrt{G_t G_r}\; e^{-j2\pi\frac{r_1+r_2}{\lambda}}\, u(t-\tau)}{r_1 + r_2}\right] e^{j2\pi fct}\right\}, \quad (2\text{-}1)$$

where

G_t : *the transmitter antenna gain,*

G_r : *the receiver antenna gain,*

λ : *the wavelength of the transmitted signal,*

R : *the reflection coefficient,*

$r_1 + r_2$: *the sum of distance of reflected path component,*

$u(t)$: *the transmitted signal.*

Different antennas with different power gains can be used for system designs. In our scenario, two omnidirectional half-wave dipole antennas with power gain of 1.64 which are placed on two different ships with some distance are used [24]. While one is used as the transmitter antenna, the other is used as the receiver antenna.

In this channel model;

- Because there are few obstacles on sea surface, the two ray channel model is enough for the communication system used in this work. So the multipath components other than the reflected signal from sea surface, if present, are assumed to be negligible and ignored.

- The delay between the direct and reflected components is neglected and the signals are assumed to arrive at the antennas at the same time [15].

- The signal and antenna variations due to ships' motions and wave motions are ignored.

- The ships are assumed to be almost stationary and the variations of signals in amplitude and/or frequency are assumed to be negligible.

The terms refraction and reflection are the two important parameters to characterize the channel. Due to bending of the signals in atmosphere, the distances that they follow should be determined correctly by taking the refraction into account. The signal that is reflected from the surface may experience some losses, so it is important to express it carefully. These issues are explained in latter sections.

2.2 REFRACTION

Because the index of refraction is not constant, electromagnetic waves are bent as they propagate as observed in Figure 2-2. The term refraction index (n) is the

property of a medium to bend an electromagnetic wave as it passes through the medium. The refraction index decreases with increasing height above the earth and it changes between 1.00025 and 1.00040 [8, 15].

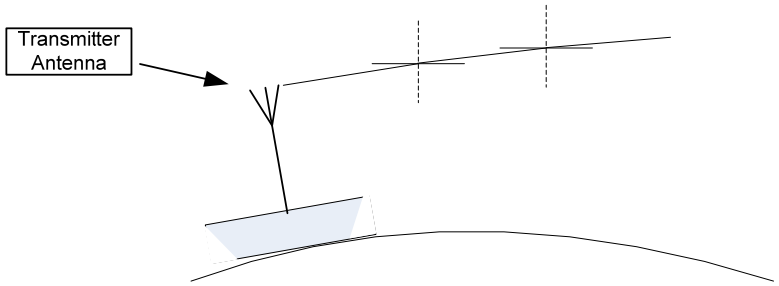

Figure 2-2: Wave bending during propagation through the medium

The term refractivity N is defined using the index of refraction as follows:

$$N = (n - 1)x10^6, \tag{2-2}$$

where

$n : the\ index\ of\ refraction,$

$N : the\ refractivity.$

The values of the minimum monthly mean value of N throughout the world have been published and the most commonly used value for N is 301 [8]. Taking the refractivity value as $N = 301$, the effective earth's radius value is obtained as follows [8]:

$$R_{eff} = R_e[1 - 0.04665\exp(0.005577N)]^{-1}, \tag{2-3}$$

where

R_{eff} : $the\ effective\ earth's\ radius$,

R_e : $the\ actual\ earth's\ radius\ \approx 6370\ km$.

Taking $R_e \approx 6370\ km$ and $N = 301$, the effective earth's radius is found as:

$$R_{eff} \approx 8500\ km\,. \tag{2-4}$$

Using the geometry and R_{eff} value the path lengths $d_1,\ r_1,\ r_2\ and\ r_d$ in Figure 2-1 can be calculated by geometry as follows [15, 21, 22]:

$$d_1 = \frac{d}{2} + \ p\cos\left(\frac{\Omega + \pi}{3}\right), \tag{2-5}$$

where

$$p = \frac{2}{\sqrt{3}}\sqrt{R_{eff}(h_t + h_r) + \left(\frac{d}{2}\right)^2},$$

$$\Omega = cos^{-1}\left|\frac{2R_{eff}(h_t - h_r)d}{p^3}\right|,$$

$$r_1 = \left[R_{eff}^2 + (R_{eff} + h_t)^2 - 2R_{eff}(R_{eff} + h_t)\cos(\frac{d_1}{R_{eff}})\right]^{1/2}, \tag{2-6}$$

$$r_2 = \left[R_{eff}^2 + (R_{eff} + h_r)^2 - 2R_{eff}(R_{eff} + h_r)\cos(\frac{d - d_1}{R_{eff}})\right]^{1/2}, \quad (2\text{-}7)$$

$$r_d = [{r_1}^2 + {r_2}^2 + 2r_1 r_2 \cos(2\Psi)]^{1/2}, \quad (2\text{-}8)$$

where

$$\Psi = cos^{-1}\left[\left(\frac{R_{eff} + h_t}{r_1}\right) + \sin(\frac{d_1}{R_{eff}})\right].$$

In our model, the path lengths are calculated with the formulas given in (2-5), (2-6), (2-7) and (2-8).

2.3 REFLECTION

In the two ray channel model, the transmitted signal follows two paths: direct path and reflected path. The signal that follows the reflected path reflects from the sea surface.

The reflected signal energy consists of specular (mirror –like reflection) and diffuse (scattering type reflection) components. When the surface is smooth only the specular component exists. When the surface is rough, diffuse component also exists and the reflected signal components that are not reflected specularly will be scattered from the rough surface at various angles in a random manner [15].

In the following sections, the specular and the diffuse components of the reflection coefficient are investigated in some detail.

2.3.1 SMOOTH SURFACE REFLECTION

When the surface is smooth, only the specular reflection coefficient is taken into consideration. The smooth surface reflection coefficient expression is expressed as follows [15, 21]:

$$\rho_0 = \Gamma D , \tag{2-9}$$

where

Γ : *the Fresnel reflection coefficient,*

D : *the divergence factor.*

The curvature of the earth has a tendency to spread out the reflected energy more than a corresponding flat surface. The spreading of the reflected energy from a curved surface to that from a flat surface is taken into consideration by introducing the divergence factor D which is given as follows [15, 21]:

$$D = \frac{reflected\ field\ from\ curved\ surface}{reflected\ field\ from\ flat\ surface},$$

$$D = \frac{r_1 + r_2}{r_1}\sqrt{\frac{\rho_1^r + \rho_2^r}{(\rho_1^r + r_2) + (\rho_2^r + r_2)}}, \tag{2-10}$$

where

ρ_1^r *and* ρ_2^r : *the principal radii of curvature of the reflected wavefront at the point of reflection,*

$$\frac{1}{\rho_1^r} = \frac{1}{r_1} + \frac{1}{\rho \sin\Psi} + \sqrt{\frac{1}{(\rho \sin\Psi)^2} - \frac{4}{{R_{eff}}^2}},$$

$$\frac{1}{\rho_2^r} = \frac{1}{r_1} + \frac{1}{\rho \sin\Psi} - \sqrt{\frac{1}{(\rho \sin\Psi)^2} - \frac{4}{{R_{eff}}^2}},$$

$$\rho = \frac{R_{eff}}{1 + (\sin\Psi)^2}.$$

The Fresnel reflection coefficients for vertical and horizontal polarizations are given as follows [15, 21]:

$$\Gamma_v = \frac{\epsilon_r \sin\Psi - \sqrt{\epsilon_r - (\cos\Psi)^2}}{\epsilon_r \sin\Psi + \sqrt{\epsilon_r - (\cos\Psi)^2}}, \tag{2-11}$$

$$\Gamma_h = \frac{\sin\Psi - \sqrt{\epsilon_r - (\cos\Psi)^2}}{\sin\Psi + \sqrt{\epsilon_r - (\cos\Psi)^2}}, \tag{2-12}$$

where

$\epsilon_r : the\ relative\ dielectric\ constant\ of\ the\ surface,$

$\Psi : the\ grazing\ angle.$

The relative dielectric constant of the surface is the ratio of the dielectric constant of the surface material to the dielectric constant of a vacuum and represented as follows [15]:

$$\epsilon_r = \epsilon_{1r} - j\epsilon_{2r}, \tag{2-13}$$

where

$\epsilon_{2r}: the\ loss\ in\ the\ material = 60\ \lambda\ \sigma,$

$\lambda: the\ wavelength,$

$\sigma: the\ conductivity.$

In our model, the conductivity $\sigma = 4.64$ and $\epsilon_{1r} = 81$ values are used for the sea surface [21].

The magnitude and phase of the Fresnel reflection coefficient are plotted in Figure 2-3 and Figure 2-4 for both horizontal and vertical polarizations at 9 GHz.

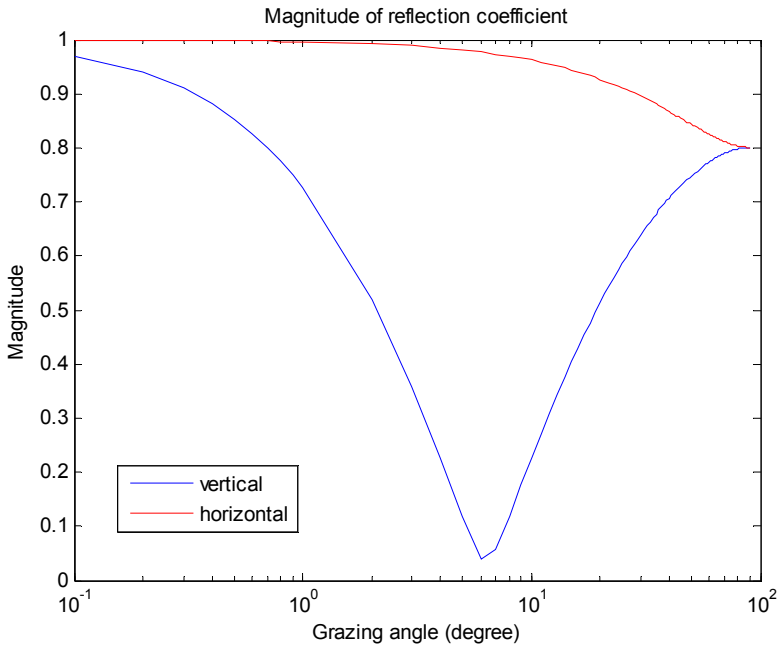

Figure 2-3: The magnitude of Fresnel reflection coefficient for horizontal and vertical polarizations

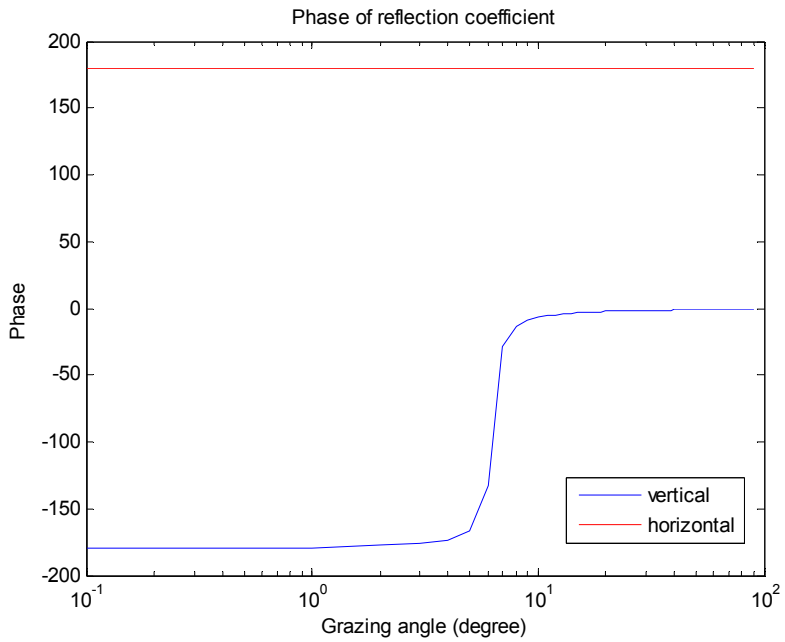

Figure 2-4: The phase of Fresnel reflection coefficient for horizontal and vertical polarizations

It is observed form the plots in Figure 2-3 and Figure 2-4 that the magnitudes of the reflection coefficient for horizontal and vertical polarizations are equal at a grazing angle of 0 and 90 degrees.

2.3.2 ROUGH SURFACE REFLECTION

When the reflection surface is not smooth, both specular and diffuse components are taken into consideration and the reflection coefficient expression becomes as follows [15]:

$$\rho = \rho_s + \rho_d \,, \tag{2-14}$$

where

$\rho_s : the\ rough\ specular\ reflection\ coefficient,$

$\rho_d : the\ rough\ diffuse\ reflection\ coefficient.$

The rough specular reflection coefficient and the rough diffuse reflection coefficient are explained in the following section.

2.3.2.1 ROUGH SPECULAR REFLECTION COEFFICIENT

For the rough surface reflection case, the magnitude of the smooth surface reflection coefficient is reduced proportional to the surface roughness and the rough specular reflection coefficient expression becomes as follows [15]:

$$\rho_s = \rho_0 R_s = \Gamma\ D\ R_s\ , \tag{2-15}$$

where

$\rho_s : the\ rough\ specular\ reflection\ coefficient,$

$R_s : the\ root\ mean\ square\ (RMS) of\ rough\ specular\ scattering\ coefficient.$

The RMS of the rough specular scattering coefficient is due to the randomness of the surface and expressed as follows [15]:

$$R_s = exp[-8\pi^2\ \delta^2]\ x\ I_0[8\pi^2\ \delta^2]\ , \tag{2-16}$$

where

$\delta : the\ roughness\ factor,$

$I_0 : the\ modified\ Bessel\ function.$

The roughness factor δ is expressed as follows [15]:

$$\delta = \frac{\sigma_h \sin\Psi}{\lambda}, \tag{2-17}$$

where

σ_h : *the standard deviation of normally distributed surface height,*

Ψ : *the grazing angle,*

λ : *the wavelength.*

The standard deviation of surface height σ_h is defined as ¼ of the significant wave heights. The significant wave height is defined as the mean wave height from trough to peak of the highest third of the waves. Considering the wave heights and sea states in Table 2-1 which are defined by World Meteorological Organization (WMO) [25], the standard deviation of surface height σ_h is taken as 1 m in this work corresponding to the sea state 5 of rough surface with 4 m peak to trough wave height.

Table 2-1: Sea state codes of WMO

WMO Sea State Code	Wave Height (m)	Descriptive Terms
0	0	Calm (glassy)
1	0 - 0.1	Calm (rippled)
2	0.1 - 0.5	Smooth (wavelets)
3	0.5 - 1.25	Slight
4	1.25 - 2.5	Moderate
5	2.5 - 4	Rough
6	4 - 6	Very rough
7	6 - 9	High
8	9 - 14	Very high
9	over 14	Phenomenal

2.3.2.2 ROUGH DIFFUSE REFLECTION COEFFICIENT

The rough diffuse reflection coefficient is expressed as follows [15]:

$$\rho_d \;=\; \rho_0 R_d = \Gamma\, D\, R_d = \Gamma\, D\, (R_{dx} + j\, R_{dy})\,, \tag{2-18}$$

where

$R_d : the\ rough\ diffuse\ scattering\ coefficient.$

The rough diffuse scattering coefficient is circularly symmetric complex Gaussian distributed, $R_{dx} \sim N(0, \sigma_d^2)$ and $R_{dy} \sim N(0, \sigma_d^2)$ and they are independent. The Rayleigh parameter σ_d is used in the model [15].

$$\sigma_d = \begin{cases} \sqrt{2}\, 3.68\, \delta & ,0 \le \delta < 0.1 \\ \sqrt{2}\, (0.454 - 0.858\, \delta\,) & ,0.1 \le \delta < 0.5 \\ \sqrt{2}\, 0.025\, \delta & ,0.5 \le \delta \end{cases}$$

where

$\delta : the\ roughness\ factor,$

$\sigma_d : the\ Rayleigh\ parameter.$

CHAPTER 3

PATH LOSS AND SHANNON CAPACITY

In this chapter, we present some results about the path loss and the channel capacity over two ray channel for sea platform links.

3.1 PATH LOSS CALCULATIONS

The path loss of the channel is the ratio of the transmitted signal power to the received signal power. Path loss is caused by the dissipation of the power radiated by the transmitter as well as effects of the propagation channel. We can compute the received power and the path loss by the formula given below [1, 2]:

$$P_r = P_t \left(\frac{\lambda}{4\pi}\right)^2 \left| \frac{\sqrt{G_t G_r}\; e^{-j2\pi \frac{r_d}{\lambda}}}{r_d} + R \frac{\sqrt{G_t G_r}\; e^{-j2\pi \frac{r_1+r_2}{\lambda}}}{r_1 + r_2} \right|^2,$$

$$PL = \frac{P_t}{P_r} = \frac{1}{\left(\left(\frac{\lambda}{4\pi}\right)^2 \left| \frac{\sqrt{G_t G_r}\; e^{-j2\pi \frac{r_d}{\lambda}}}{r_d} + R \frac{\sqrt{G_t G_r}\; e^{-j2\pi \frac{r_1+r_2}{\lambda}}}{r_1 + r_2} \right|^2 \right)}, \qquad (3\text{-}1)$$

where

P_t : *the transmitted signal power,*

P_r : $the\ received\ signal\ power$,

PL : $the\ path\ loss\ of\ the\ channel$,

G_t : $the\ transmitter\ antenna\ gain$,

G_r : $the\ receiver\ antenna\ gain$,

λ : $the\ wavelength\ of\ the\ transmitted\ signal$,

R : $the\ reflection\ coefficient$,

$r_1 + r_2$: $the\ sum\ of\ distance\ of\ reflected\ path\ component$,

r_d : $the\ direct\ path\ distance$,

c : $the\ speed\ of\ light\ = 3x10^8\ m/s$,

f : $the\ frequency\ of\ the\ transmitted\ signal$.

Using the two ray channel model and the parameters in Table 3-1 and the path loss plots in Figure 3-1 and Figure 3-2 are obtained using the path loss formula in (3-1).

Table 3-1: Parameters of the system in Figure 3-1 and Figure 3-2

Parameter		**Value**
Path loss formula		Formula in (3-1)
Transmitter antenna height	h_t	50 m
Receiver antenna height	h_r	30 m
Transmitter antenna gain	G_t	1.64
Receiver antenna gain	G_r	1.64
Reflection		Rough surface- Only specular part
Polarization		Horizontal & Vertical
Frequency	f	1 GHz 2 GHz 5 GHz

Figure 3-1 and Figure 3-2 depict the path loss as a function of distance and center frequency for horizontal and vertical polarizations, respectively.

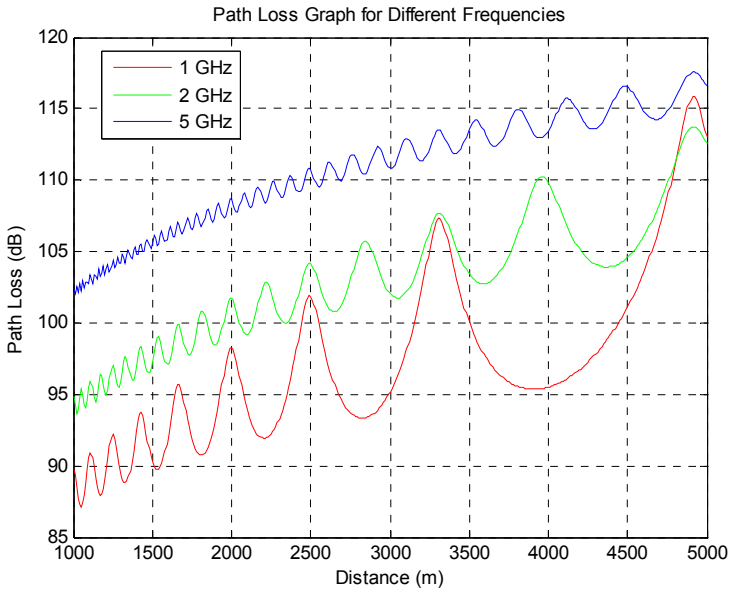

Figure 3-1: Path loss graph for different frequencies for horizontal polarization

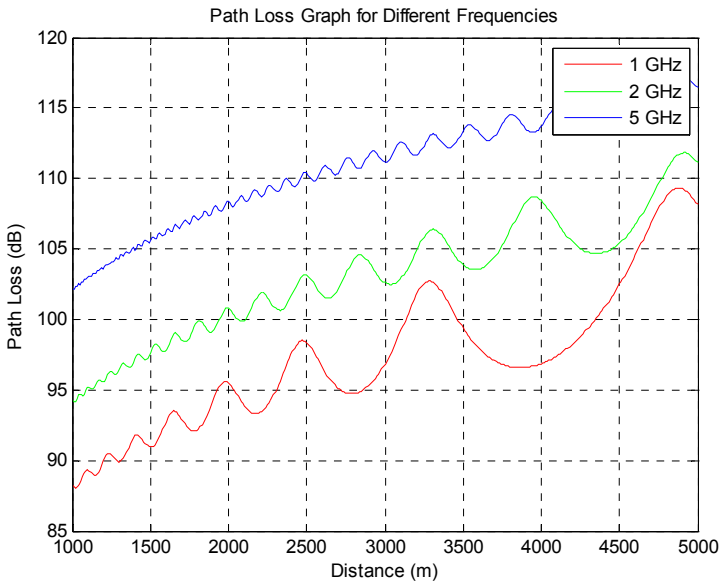

Figure 3-2: Path loss graph for different frequencies for vertical polarization

The following observations can be done from the plots in Figure 3-1 and Figure 3-2:

- The path loss is frequency dependent. As the frequency of the transmitted signal is increased the path loss value increases in general.

- As the distance between the transmitter and the receiver antennas changes, oscillations occur in path loss graphs. These oscillations are due to the destructive and constructive effects of the received signal from direct path and reflected path.

- Because the magnitude of the reflection coefficient for horizontal polarization is higher than the reflection coefficient for vertical polarization at low grazing angles, the effect of reflected path signal becomes more effective for horizontal polarization case and the oscillations are more severe for the horizontal polarization case in path loss plots.

3.2 SHANNON CAPACITY

In this section, we bind our findings in Section 3.1 to the feasible communication rates by the aid of channel capacity formula. The famous channel capacity formula was found by Claude Shannon in 1948's. Shannon derived the channel capacity from the mutual information maximized over all possible input distributions. Shannon's coding theorem and its converse proved that a code exists that could achieve a data rate close to capacity with negligible probability of error [2]. This means that if the information rate R is less than channel capacity C, small error probabilities can be obtained using coding and modulation techniques.

Shannon's capacity formula is applicable to band limited AWGN waveform channels with a band limited and average power limited input. This theorem states that the capacity of a continuous channel of bandwidth W (Hz), with band limited white Gaussian noise of power spectral density $N_0/2$, is given by the formula [3, 4]:

$$C = W\ log_2\left(1 + \frac{P_{av}}{W\ N_0}\right) \qquad (bits/s), \tag{3-2}$$

where

$C : the\ capacity\ of\ the\ channel,$

$W : the\ channel\ bandwidth,$

$P_{av} : the\ average\ received\ signal\ power,$

$N_0 :\ the\ single\ sided\ noise\ power\ density.$

The noise power can be expressed as follows [24]:

$$N = noise\ power = N_0\, W = (k\, T_{sys})\, W\ , \tag{3-3}$$

where

$k : the\ Boltzman\ constant = 1.38\ x10^{-23}\ \frac{J}{K}$,

$T_{sys} : (273 + T)\ Kelvin =\ the\ sum\ of\ the\ noise\ temperature\ of\ the$

$antenna\ and\ the\ effective\ input\ noise\ temperature\ of\ overall\ receiving$

$system,$

$W : the\ channel\ bandwidth.$

During this work, the overall system temperature value T_{sys} is taken as 300^{o} K.

It is obvious from the formula in (3-2) that, for a fixed bandwidth, the channel capacity increases with increasing transmitted power and signal to noise ratio.

Channel bandwidth is an important constraint that affects the value of channel capacity. For fixed transmitted power, the capacity can be increased by increasing the bandwidth. However increase in channel bandwidth leads to an increase in noise power also. So the capacity curve approaches the asymptotic value:

$$C = \frac{P_{av}}{N_0}\ log_2 e \qquad (bits/s) \tag{3-4}$$

as the bandwidth approaches infinity [4],

where

C : *the capacity of the channel,*

P_{av} : *the average received signal power.*

In Figure 3-3, using the two ray channel model, the capacity curves are obtained with respect to the changing transmitted power for 2 MHz, 5 MHz and 10 MHz channel bandwidths at 10 GHz frequency at a distance of 10 km using the equation in (3-2) for horizontal polarization.

In Figure 3-4, using the two ray channel model, the capacity curve is obtained as a function of bandwidth for a fixed transmitted power of 1 watt. The plot is obtained at 10 GHz frequency for a distance of 10 km. Also the asymptotic value of the capacity curve in (3-4) is plotted.

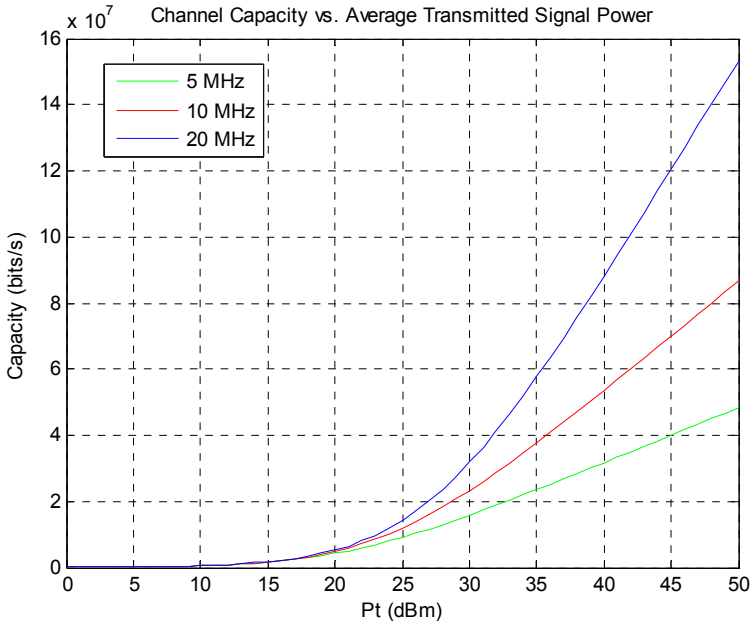

Figure 3-3: Channel capacity for different bandwidths

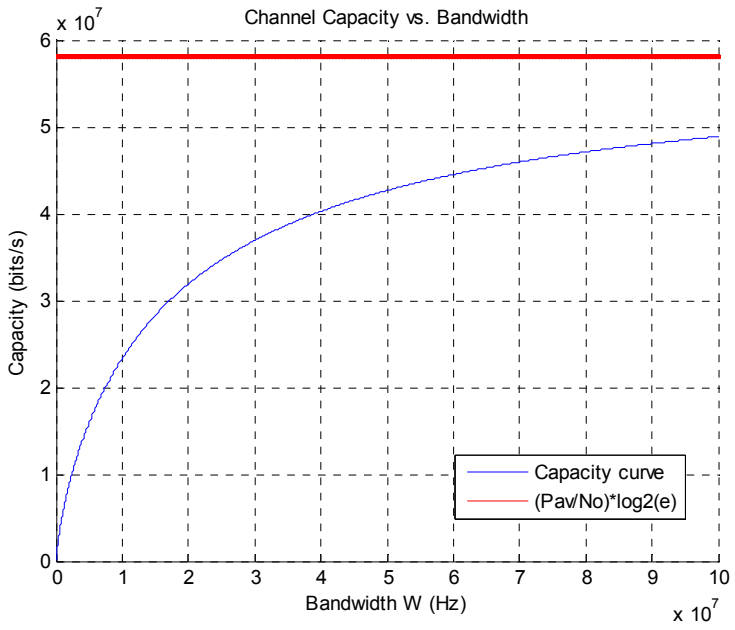

Figure 3-4: Channel capacity as a function of bandwidth for a fixed transmitted power

When the diffuse component of the reflection coefficient is also taken into account, because of the randomness of the diffuse component of the reflection coefficient, we obtain a different result at each experiment. For that purpose, it is needed to conduct the experiment for several times. A scatter plot depicting the capacity distribution is shown in Figure 3-5, with the parameters in Table 3-2.

Table 3-2: Parameters of plot in Figure 3-5

Parameter		**Value**
Distance	d	5 km
Frequency	f	5 GHz
Bandwidth	W	5 MHz
Transmitter antenna height	h_t	50 m
Receiver antenna height	h_r	30 m
Transmitter antenna gain	G_t	1.64
Receiver antenna gain	G_r	1.64
Transmitted power	P_t	1 watt

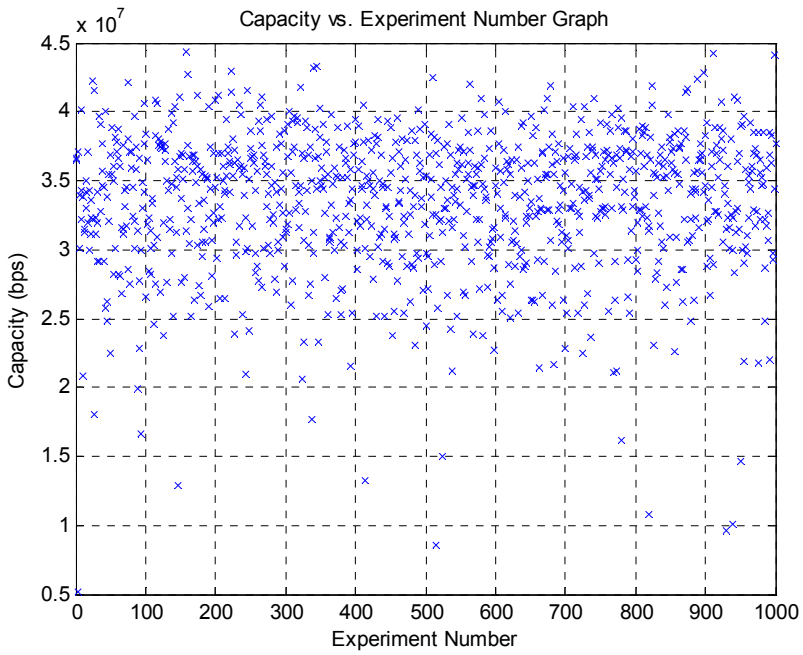

Figure 3-5: Capacity vs. experiment number graph

With the results shown in Figure 3-5, the histogram graph in Figure 3-6 is constructed. It shows that the total occurrence number of each capacity value. From the graph in Figure 3-6, we may get some useful conclusions as written in Table 3-3, such as the mean capacity, standard deviation, variance and probability of obtaining the capacity value in some interval.

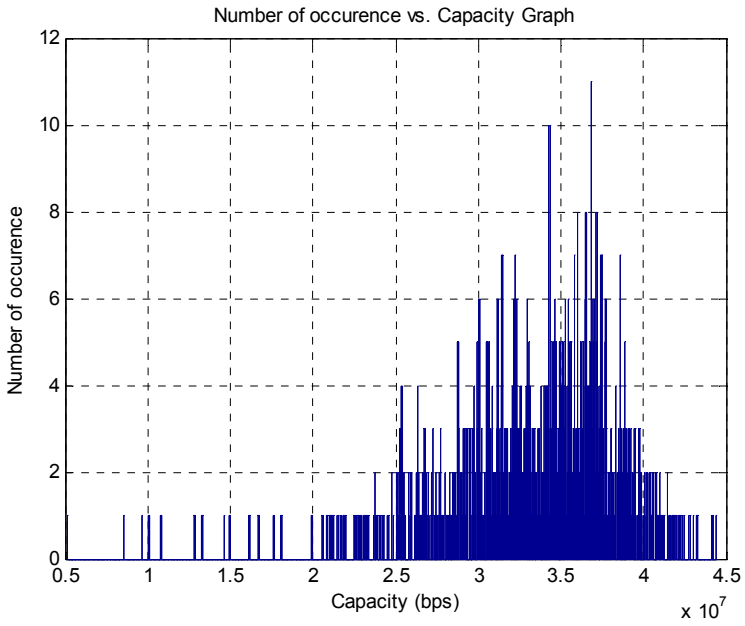

Figure 3-6: Number of occurrence vs. capacity graph

Table 3-3: Results of the system in Figure 3-6

Parameter	**Value**
Mean capacity	33 Mbps
Variance	25 $(\text{Mbps})^2$
Standard deviation	5 Mbps
Probability that capacity value is between 30 Mbps and 35 Mbps	0.34

CHAPTER 4

FREQUENCY DIVERSITY AND DIVERSITY COMBINING TECHNIQUES

In a multipath communication channel, the signal components of different paths go under different attenuation, distortion, phase shifts and time delays [5]. These effects which may sometimes be constructive and sometimes destructive, cause fading. In order to overcome the fading effect, diversity techniques can be used. In this chapter, diversity techniques are reviewed, and for the two path sea channel model coherence bandwidth analysis is provided.

4.1 DIVERSITY TECHNIQUES

In a communication system suffering from multipath fading, in order to increase the system performance, different diversity techniques can be used. The main aim of diversity techniques is transmitting and/or receiving the signal with several copies. Because the copies of these transmitted signal undergoes different fading such as attenuation, distortion, phase and time delays; when one of these signal may go under deep fading, others may not [5]. By that principle, the performance of the system is expected to be increased. In almost all diversity techniques, diversity decisions are made by the receiver and are unknown by the transmitter [3]. There are mainly the following diversity techniques that are used in communication systems:

- *Space Diversity*

- *Time Diversity*
- *Polarization Diversity*
- *Frequency Diversity*

The operation principles, advantages and disadvantages of different diversity techniques are explained briefly in this chapter.

4.1.1 SPACE DIVERSITY

Space diversity, also called antenna diversity, techniques can be efficiently used in fading channels. The main idea of this technique is transmitting and/or receiving the desired signal with more than one antenna as given in Figure 4-1. By spacing the antennas far enough apart, changing the antenna number and using array combinations different received signals may go under independent fading [3, 5, 8]. A system example for space diversity technique with one transmitting antenna and several receiving antennas can be seen from the scheme given in Figure 4-1.

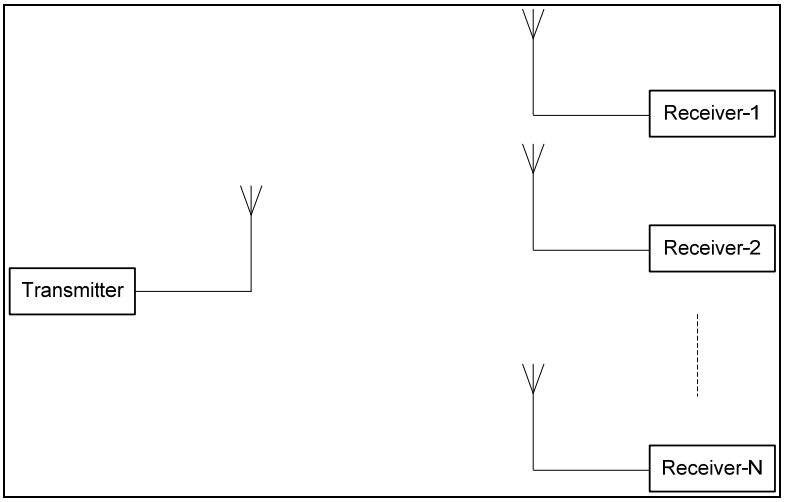

Figure 4-1: Space diversity

Although the application of space diversity technique does not require additional frequency spectrum and transmission time, the additional antennas may constrain its applications on physical medium [5, 8].

4.1.2 TIME DIVERSITY

Another diversity approach in fading channel is time diversity. Transmitting the desired signal in different periods of time is the main application idea of the time diversity technique. When the signals are transmitted with enough time periods, the signals are received with independent fading conditions which provide diversity [3, 5]. The working principle of time diversity technique may be seen from the scheme given in Figure 4-2.

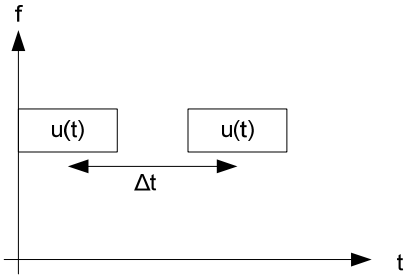

Figure 4-2: Time diversity

4.1.3 POLARIZATION DIVERSITY

Polarization diversity technique can be considered as a special case of space diversity, because separate antennas are used. There is no need of large antenna separations as in the case of space diversity, for that reason polarization diversity is more practical than space diversity [3].

The signals on different polarizations have uncorrelated fading statistics. Therefore, these signals may be used in diversity systems. Since there are only two orthogonal polarizations, there are two diversity branches. In addition, there is a 3 dB loss in signal, because the transmitted signal power is divided between two transmitting antennas [8].

4.1.4 FREQUENCY DIVERSITY

In frequency diversity, the signals are transmitted on different carrier frequencies. A simple frequency working principle scheme is given in Figure 4-3. The signals at different frequencies can be combined with different combining techniques at the receiver. Different combining techniques may result in different system performances and depending on the combining technique on receiver side, the performance of the system is expected to be increased.

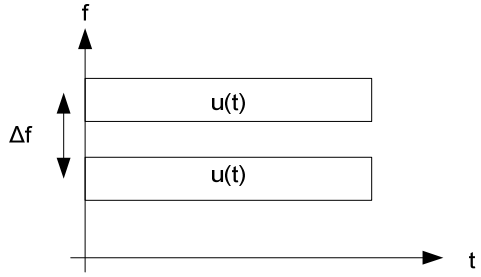

Figure 4-3: Frequency diversity

The success of frequency diversity technique depends on the correlation degree of different diversity branches. The frequencies that are separated at least one coherence bandwidth will be uncorrelated [14]. That's why coherence bandwidth is an important parameter for the frequency diversity applications to obtain independent signals.

The frequency diversity technique is often used in microwave line of sight links which carry several channels in Frequency Division Multiplexing (FDM) mode due to deep fading effects [3].

Another advantage of frequency diversity is the reduction of the number of antennas to one at each end of the path [8]. Although frequency diversity provides considerable system performance improvement, the main disadvantages of this technique are the use of wider frequency band and the use many transmitters and receivers at transmitter and receiver sides [3].

In our model, we use a single antenna at each end of the system to eliminate time variations. In following section, coherence bandwidth parameter is described.

4.2 COHERENCE BANDWIDTH

The signal components follow different paths in a multipath channel and they arrive at the receiver with varying amplitudes, phases and time delays [7, 13]. Different time delays in different path components that make up the total field cause the statistical properties of signals of different frequencies to become essentially independent if their frequency separation is large enough [8, 11]. This frequency separation is called *"coherence bandwidth"* of the radio channel.

From another point of view, coherence bandwidth is a statistical measure of range of frequencies over which the channel can be considered "flat". The signals with frequency separation greater than coherence bandwidth are affected differently by the channel [3, 9].

Coherence bandwidth of the channel is also an important parameter for multicarrier systems, Frequency Hopping Spread Spectrum (FHSS) systems and Orthogonal Frequency Multiplexing (OFDM). Choosing the carrier spacing or frequency hop distance large enough will lead to lower fading impairment rates [7].

The analytic expression of the coherence bandwidth was first studied by Jakes, where he revealed that coherence bandwidth of the channel is inversely proportional to its rms delay spread [8, 9]. After his studies, a lot of experiments and measurements were conducted to determine the coherence bandwidth. An empirical formula is expressed in [3, 9] by expressing the coherence bandwidth in terms of rms delay spread with the threshold value of frequency correlation coefficient.

$$Bc \approx \begin{cases} \frac{1}{50\sigma_r}, & if\ \eta_o = 0.9 \\ \frac{1}{5\sigma_r}, & if\ \eta_o = 0.5 \end{cases} \quad (4\text{-}1)$$

where

$\sigma_r : the\ rms\ delay\ spread,$

$\eta_o : the\ frequency\ correlation\ function.$

The frequency correlation function is a measure of the magnitude of correlation between the channel responses at two spaced frequencies. No single definitive value of correlation has emerged for the specification of the coherence bandwidth, hence the coherence bandwidth is defined for different correlation coefficients (0.5 and 0.9) that are evaluated from correlation coefficient function [10].

Although the formula given in (4-1) is obviously not an exact expression for coherence bandwidth, it gives an idea about characterization of the channel [3, 12].

The mean excess delay is defined as the first moment of the power delay profile and expressed as follows [3, 10]:

$$\bar{\tau} = \frac{\sum_k {\alpha_k}^2 \tau_k}{\sum_k {\alpha_k}^2} = \frac{\sum_k P(\tau_k)\tau_k}{\sum_k P(\tau_k)}\ , \quad (4\text{-}2)$$

where

$\bar{\tau} : the\ mean\ excess\ delay,$

${\alpha_k}^2 = P(\tau_k) : the\ power\ of\ the\ k^{th}\ path\ signal,$

$\tau_k : time\ difference\ between\ two\ signal\ following\ different\ paths.$

The rms delay spread is defined as the square root of the second central moment of the power delay profile and expressed as follows:

$$\sigma_r = \sqrt{\overline{\tau^2} - \bar{\tau}^2}\,, \tag{4-3}$$

where

$\sigma_r : the\ rms\ delay\ spread,$

$$\overline{\tau^2} = \frac{\sum_k {\alpha_k}^2 {\tau_k}^2}{\sum_k {\alpha_k}^2} = \frac{\sum_k P(\tau_k) {\tau_k}^2}{\sum_k P(\tau_k)}, \tag{4-4}$$

${\alpha_k}^2 = P(\tau_k) : the\ power\ of\ the\ k^{th}\ \ path\ signal.$

The equations in (4-2) and (4-4) do not rely on the absolute power level of $P(\tau_k)$, but only the relative amplitudes of multipath components within $P(\tau_k)$ [3].

In our case, because we have only two different paths, the following delay spread expression is used:

$$\tau_k = \frac{r_r - r_d}{c}\ (\text{sec})\,, \tag{4-5}$$

where

$r_r : the\ path\ length\ of\ the\ signal\ that\ follows\ reflected\ path\ (m),$

$r_d : the\ path\ length\ of\ the\ signal\ that\ follows\ direct\ path\ (m),$

$c : the\ speed\ of\ light\ (m/\text{sec}).$

In Figure 4-4 and Figure 4-5, the coherence bandwidth of the channel is plotted as a function of distance using the expression given in (4-3) for the case of correlation coefficient $\eta_o = 0.5$ and $\eta_o = 0.9$, 5 Ghz frequency and horizontal polarization.

The values in Figure 4-4 are 10 times greater than the values in Figure 4-5 due to the definition given in (4-1).

As observed from the plots in Figure 4-4 and Figure 4-5, when the distance between antennas is increased, coherence bandwidth increases. This means that, signals have greater correlation at long distance and the benefit owing to the use of frequency diversity is likely to be reduced at long distance [14].

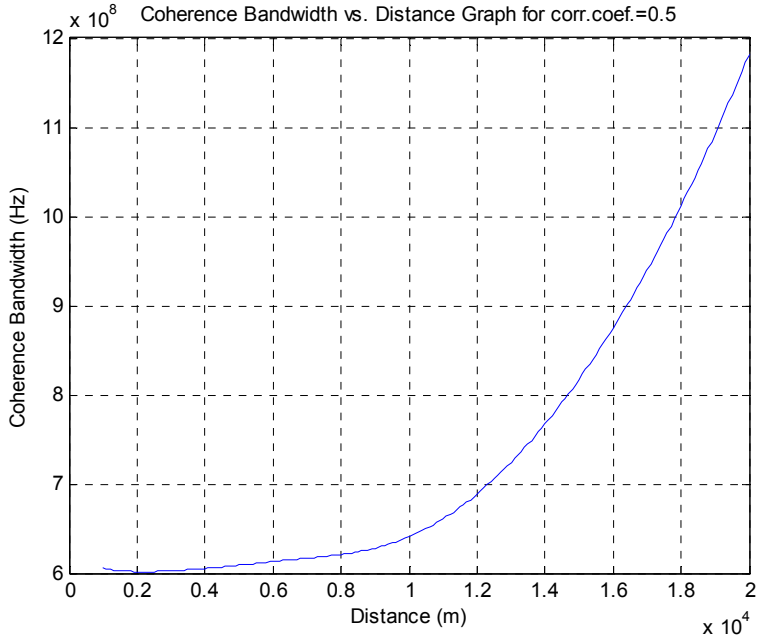

Figure 4-4: Coherence bandwidth vs. distance graph for corr coef=0.5 at 5 GHz

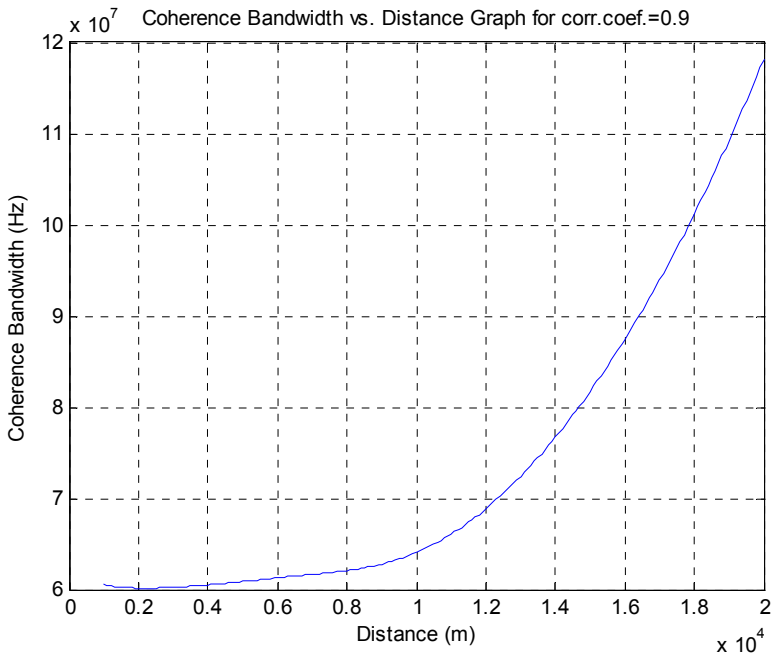

Figure 4-5: Coherence bandwidth vs. distance graph for corr coef=0.9 at 5 GHz

4.3 DIVERSITY COMBINING TECHNIQUES

There are mainly the following combining techniques in literature that are used at the receiver side in order to overcome the effects of different fading characteristics of different signals:

- *Selection Switching (SS)*
- *Maximal Ratio Combining (MRC)*
- *Equal Gain Combining (EGC)*

In terms of maximizing the SNR, the optimal technique is the Maximum Ratio Combining (MRC) technique.

The receiver whose block diagram is shown in Figure 4-6 is used for general linear combiner type diversity reception.

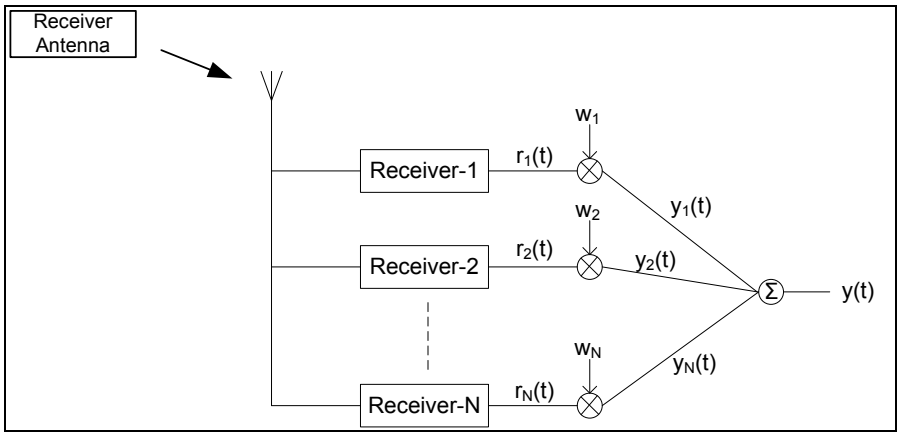

Figure 4-6: Receiver block diagram for diversity techniques

In block diagram in Figure 4-6, the received signal for each diversity branch is expressed as follows:

$$r_k(t) = \alpha_k e^{j\theta_k} u(t) \; + \; n_k(t)\,, \tag{4-6}$$

where

$r_k(t)$: *the received signal component with* k^{th} *frequency*,

$\alpha_k e^{j\theta_k}$: *the complex channel attenuation of signal at the* k^{th} *frequency*,

$u(t)$: *the transmitted signal*,

$n_k(t)$: *AWGN at the* k^{th} *frequency*,

k : *the index of a diversity branch* $= 1 \ldots N$,

N : *the total number of diversity branches*.

The received signals are weighted with coefficients w_k for a certain diversity combining technique. The weighted signal is expressed as follows:

$$y_k(t) = w_k\, r_k(t), \tag{4-7}$$

where

$y_k(t) : the\ weighted\ received\ signal\ at\ the\ k^{th}\ frequency,$

$r_k(t) : the\ received\ signal\ at\ the\ k^{th}\ frequency,$

$w_k : the\ weight\ coefficient.$

After the received signal components are weighted, they are summed together and different system improvements are obtained with respect to the diversity combining technique used.

In the following sections, different combining techniques are examined by using the receiver block diagram in Figure 4-6 by using the expressions in (4-6) and (4-7) in terms of their system performances.

4.3.1 SELECTION SWITCHING

Selection switching method is the simplest method within other diversity combining methods. Basic block diagram of selection switching method is given in Figure 4-7 [5].

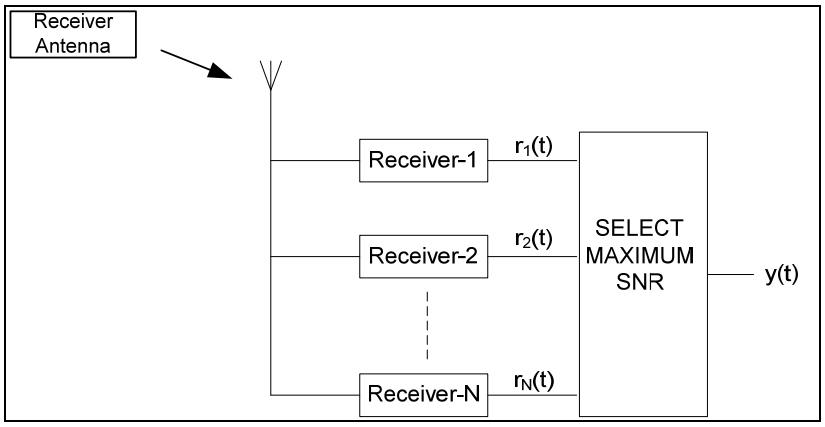

Figure 4-7: Block diagram of selection switching

The receiver chooses the signal component with maximum signal to noise ratio (SNR) and it is connected to the output for selection switching. The weights are chosen as follows:

$$w_k = \begin{cases} 1, & \gamma_t = max_k(\gamma_k) \\ 0, & otherwise \end{cases} \tag{4-8}$$

where

$w_k : the\ weight\ coefficient,$

$\gamma_t : the\ resultant\ SNR\ at\ the\ output\ of\ combiner,$

$\gamma_k : the\ SNR\ of\ each\ diversity\ branch.$

Then the resultant SNR becomes as follows [5, 15]:

$$\gamma_t = max_k(\gamma_k)\,, \tag{4-9}$$

where

$\gamma_t : the\ resultant\ SNR\ at\ the\ output\ of\ combiner,$

$\gamma_k : the\ SNR\ of\ each\ diversity\ branch,$

$k : The\ index\ of\ a\ diversity\ branch = 1 \ldots N\,,$

$N : the\ total\ number\ of\ diversity\ branches.$

Using the channel capacity expression given in (3-2) and the expressions given in (4-8) and (4-9), the capacity expression for selection switching technique can be expressed as follows:

$$C = W\ log_2(1 + \gamma_t) \qquad (bits/s), \tag{4-10}$$

where

C : $the\ channel\ capacity,$

W : $the\ channel\ bandwidth,$

γ_t : $the\ resultant\ SNR\ at\ the\ output\ of\ combiner.$

Although selection switching method provides some improvement, because it uses only one out of N diversity branches and ignore others; so it will not be the optimum.

4.3.2 MAXIMAL RATIO COMBINING

The block diagram of maximum ratio combiner is given in Figure 4-8. The weight coefficients w_k in maximal ratio combining method are chosen to be the complex conjugate of each received diversity branches to provide optimal SNR and it is expressed as follows [3,5]:

$$w_k = \alpha_k e^{-j\theta_k}\,, \tag{4-11}$$

where

$\alpha_k e^{-j\theta_k}$: $the\ complex\ conjugate\ of\ channel\ attenuation\ of\ signal\ at\ the\ k^{th}\ frequency.$

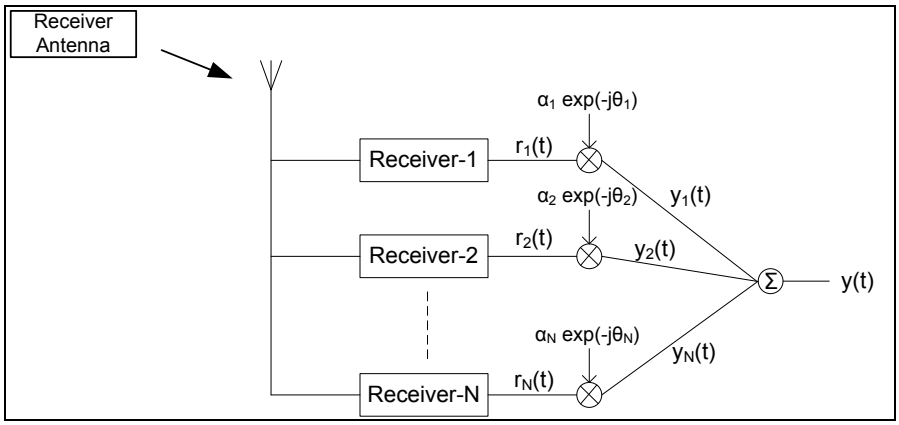

Figure 4-8: Block diagram of maximal ratio combiner

The received signal after being weighted and summed at the maximal ratio combiner, the resultant signal may be obtained as follows:

$$y_k(t) = w_k\, r_k(t)\,,$$

$$y_k(t) = (\alpha_k e^{-j\theta_k}) r_k(t)\,,$$

$$y_k(t) = (\alpha_k e^{-j\theta_k})(\alpha_k e^{j\theta_k}\, u(t) + n_k(t))\,,$$

$$y_k(t) = \alpha_k^2 u(t) + \alpha_k e^{-j\theta_k} n_k(t)\,,$$

$$y(t) = \sum_k \alpha_k^2 u(t) + \sum_k \alpha_k e^{-j\theta_k} n_k(t)\,, \tag{4-12}$$

where

$y(t) : the\ signal\ at\ the\ output\ of\ the\ combiner,$

$u(t) : the\ transmitted\ signal,$

$n_k(t) : the\ AWGN\ of\ signal\ at\ the\ k^{th}\ frequency.$

The resultant SNR value for MRC is obtained as follows:

$$P_{ys} = \left|\sum_k w_k \alpha_k e^{j\theta_k}\right|^2 P_u = \left|\sum_k \alpha_k^2\right|^2 P_u ,$$

$$P_{yn} = \left|\sum_k w_k\right|^2 P_n = \left|\sum_k \alpha_k^2\right| P_n ,$$

$$\gamma_t = \frac{P_{ys}}{P_{yn}} = \frac{|\sum_k \alpha_k^2|^2 P_u}{|\sum_k \alpha_k^2| P_n} = \left|\sum_k \alpha_k^2\right| \frac{P_u}{P_n} = \sum_k \gamma_k , \qquad (4\text{-}13)$$

where

γ_t : *the resultant SNR at the output of combiner,*

P_{ys} : *the signal power of the combined signal,*

P_{yn} : *the noise power of the combined signal,*

P_u : *the power of the signal* $u(t)$,

P_n : *the noise power of each diversity branch* (*assumed equal for each branch*),

γ_k : *the SNR of each diversity branch.*

It is observed that resultant SNR is the sum of SNR values of each diversity branch [3, 5, 8].

Using the expression given in (4-13), capacity expression is obtained as follows:

$$\mathrm{C} = \mathrm{W}\, log_2(1 + \gamma_t) = \mathrm{W}\, log_2\left(1 + \sum_k \gamma_k\right) \quad (\text{bits/s}), \qquad (4\text{-}14)$$

where

$C : the\ channel\ capacity,$

$W : the\ channel\ bandwidth,$

$\gamma_t : the\ resultant\ SNR\ at\ the\ output\ of\ combiner.$

Maximal ratio combiner is the optimal combining technique among other combining techniques. A detailed comparison of MRC with other techniques is given in Section 4.4.

4.3.3 EQUAL GAIN COMBINING

Another diversity combining method is the Equal Gain Combining (EGC). The block diagram of this technique is given in Figure 4-9. In equal gain combining method, the received signals are co-phased by choosing the weight coefficients w_k as follows:

$$w_k = e^{-j\theta_k}, \tag{4-15}$$

where

$e^{-j\theta_k} : the\ conjugate\ of\ signal\ phase\ at\ the\ k^{th}\ frequency.$

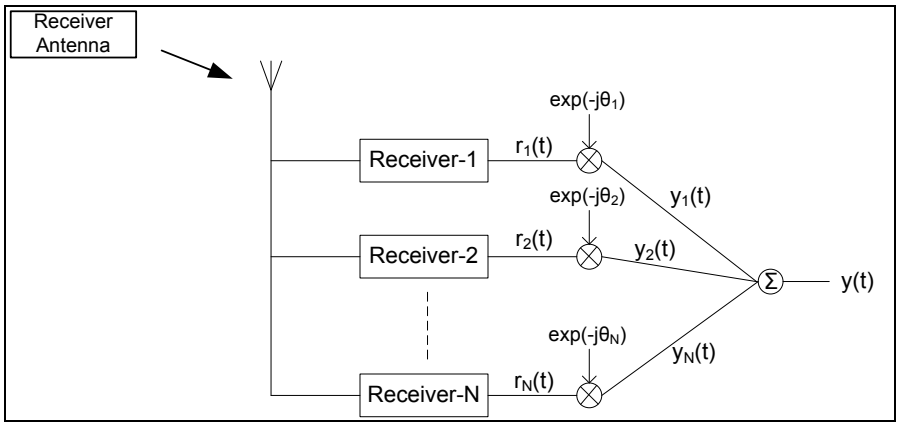

Figure 4-9: Block diagram of equal gain combiner

The received signal after being weighted and summed at the equal gain combiner, the resultant signal may be obtained as follows:

$$y_k(t) = w_k\, r_k(t)\,,$$

$$y_k(t) = (e^{-j\theta_k}) r_k(t)\,,$$

$$y_k(t) = (e^{-j\theta_k})(\alpha_k e^{j\theta_k}\, u(t) + n_k(t))\,,$$

$$y_k(t) = \alpha_k u(t) + e^{-j\theta_k} n_k(t)\,,$$

$$y(t) = \sum_k \alpha_k u(t) + \sum_k e^{-j\theta_k} n_k(t)\,, \tag{4-16}$$

where

$y(t)$: *the signal at the output of the combiner,*

$u(t)$: *the transmitted signal,*

$n_k(t)$: *the AWGN of signal at the* k^{th} *frequency.*

The resultant SNR value for EGC is obtained as follows:

$$P_{ys} = \left|\sum_k w_k \alpha_k e^{j\theta_k}\right|^2 P_u = \left|\sum_k \alpha_k\right|^2 P_u\,,$$

$$P_{yn} = \left|\sum_k w_k\right|^2 P_n = N\, P_n\,,$$

$$\gamma_t = \frac{P_{ys}}{P_{yn}} = \frac{|\sum_k \alpha_k|^2 P_u}{N\, P_n} = \left|\sum_k \alpha_k\right|^2 \frac{P_u}{N\, P_n}\,, \tag{4-17}$$

where

γ_t : *the resultant SNR at the output of combiner,*

P_{ys} : *the signal power of the combined signal,*

P_{yn} : *the noise power of the combined signal,*

P_u : *the power of the signal* $u(t)$,

P_n : *the noise power of each diversity branch* (*assumed equal for each branch*).

Using the expression in (4-17), the capacity expression is obtained as follows:

$$C = W\ log_2(1+\gamma_t) = W * log_2\left(1+\left|\sum_k \alpha_k\right|^2 \frac{P_u}{N\ P_n}\right) \quad (bits/s)\,, \qquad (4\text{-}18)$$

where

C : *the channel capacity,*

W : *the channel bandwidth,*

γ_t : *the resultant SNR at the output of combiner.*

4.4 COMPARISON OF DIVERSITY COMBINING TECHNIQUES

In this section, the advantages and disadvantages of diversity techniques which are described in previous section are explained.

- Among the combining techniques, MRC has the best performance with highest complexity under independent fading channels, on the other hand SS has the lowest performance with least complexity [5].

- Although SS is easy to implement, it is not an optimal diversity technique because it does not use all of the possible diversity branches simultaneously. SS method omits all branches except the one with highest SNR value [3].
- MRC is the optimal combining technique because it uses each of N branches in a co-phased and weighted manner such that the highest available SNR is available at the receiver at all times [3].
- Unlike the MRC, the channel gain estimate is not required in EGC [3].

In this part, a detailed comparison of diversity combining techniques is given with the following specifications:

- The two ray channel model which is defined in Chapter-2 is used as the channel model. In this model, two ships are placed with distances of 9 and 12 km between and the results obtained for 9 km and 12 km distances are plotted. Since typically the grazing angles are very low, polarization is not much important.
- Two omnidirectional half-wave dipole antennas with power gain of 1.64 which are placed on ships as transmitter and receiver antennas are used. The transmitter and receiver antenna heights are chosen as 50 m and 30 m, respectively. The channel geometry which is used for comparison of diversity combining techniques is given in Figure 4-10.

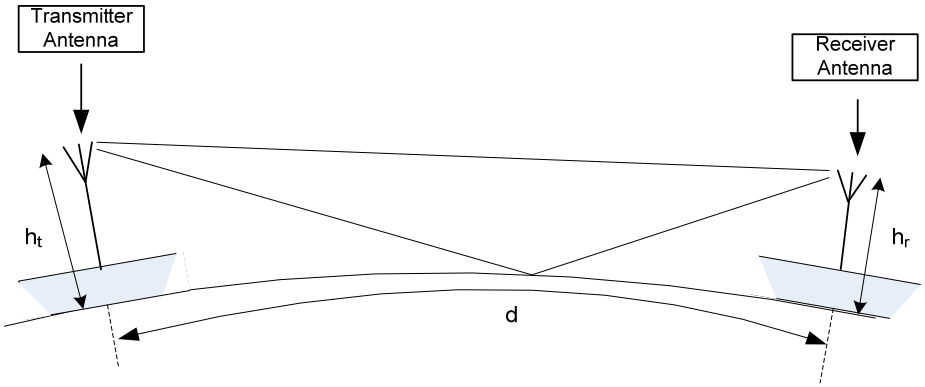

Figure 4-10: The geometry of two ray channel model

- The standard deviation of surface height σ_h is taken as 1 m, corresponding to the sea state-5 of rough surface.
- Both specular and diffuse components of the reflection coefficients are used. Due to the randomness of the diffuse component of the rough surface reflection coefficient, the experiment is repeated 1000 times. The capacity values obtained for each experiment are averaged to get the mean capacity.
- Frequency diversity is used with different number of diversity branches. The capacity curves are obtained using different diversity combining techniques for 2, 3 and 5 diversity branches and the obtained results are compared.
- The capacity curves are plotted with respect to the frequency separation between branches to see the effect of frequency separation on the system performance. In addition, frequency separation is chosen in a wide range (0-700 MHz) so that frequency separation is at least one coherence bandwidth.
- The transmission and reception is done with single antennas at both the transmitter and the receiver sides. The different diversity branches are combined and it is assumed that the signals are sent and received at the same time. The time difference between branches is neglected. The block diagram of the system for 2 branches case is shown in Figure 4-11. The diagrams for 3 and 5 branches case will be similar to the one for 2 branches case.

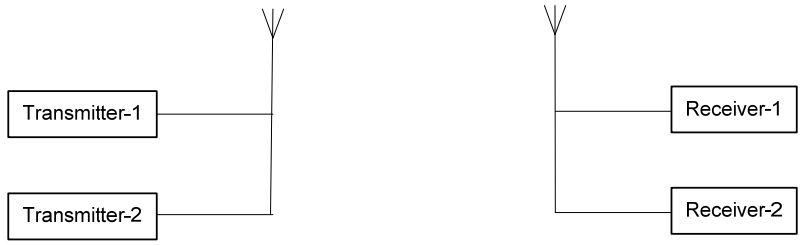

Figure 4-11: The transmitter and receiver block diagram of frequency diversity technique for 2 branches

- The total transmitted power is kept constant while obtaining the results. For one scenario, the transmitted power is decided as 1 watt. This value is divided between diversity branches. As the number of branches increases, transmitted power of each branch decreases. For example, while the transmitted power is 0.5 watt for each of 2 branches case, it is 0.2 watt for each of 5 branches case.
- The performances of diversity combining techniques, namely Selection Switching (SS), Maximal Ratio Combining (MRC) and Equal Gain Combining (EGC), are compared for different number of diversity branches. The capacity curves are obtained using expressions in (4-10), (4-14) and (4-18).
- The parameters which are used for the comparison of diversity combining techniques are summarized in Table 4-1.

Table 4-1: Parameters for comparison of combining techniques

Parameter		**Value**
Distance	d	9 km and 12 km
Transmitter antenna height	h_t	50 m
Receiver antenna height	h_r	30 m
Transmitter antenna gain	G_t	1.64
Receiver antenna gain	G_r	1.64
Bandwidth	W	5 MHz
Number of experiments	-	1000
Transmitted power	P_t	1 Watt
Number of transmitted signals	N	1, 2, 3, 5
Frequency separation between signals	Δf	0 to 700 MHz
Frequency	*N=1*	5 GHz
	N=2	5 GHz
		5 GHz−Δf
	N=3	5 GHz
		5 GHz−Δf
		5 GHz+Δf
	N=5	5 GHz
		5 GHz−Δf
		5 GHz+Δf
		5 GHz−2Δf
		5 GHz+2Δf

In Figure 4-12, the capacity values are plotted with respect to the frequency separation between 2 diversity branches. For the example, in Figure 4-12, two diversity branches have the carrier frequencies of 5 GHz and (5 GHz−Δf) where Δf is the frequency separation between diversity branches. For comparison, capacity value obtained using one carrier frequency (no diversity case) is also given.

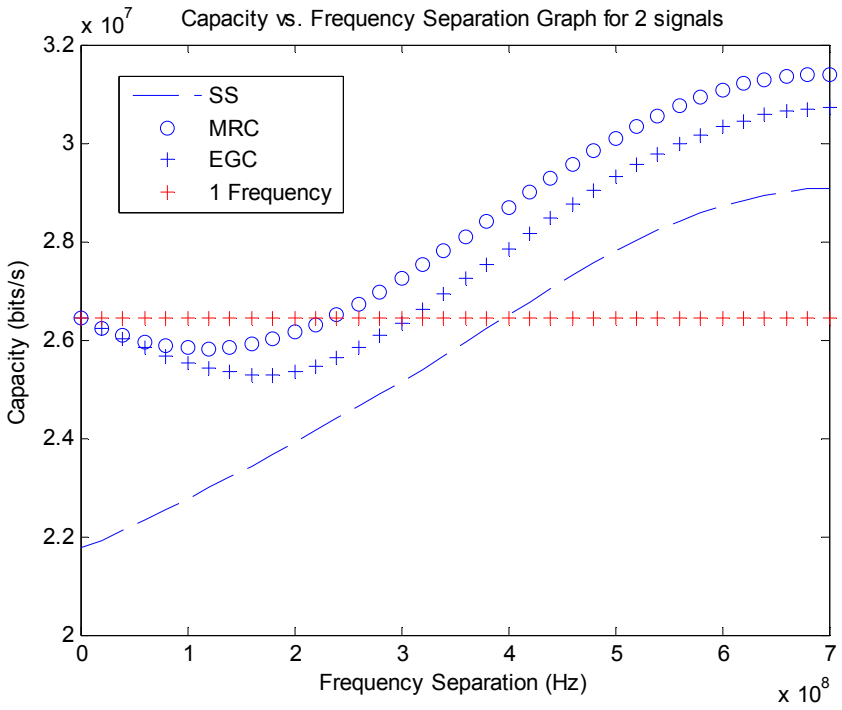

Figure 4-12: Capacity vs frequency separation graph for 2 branches for 9 km

In this case, the plot obtained for one frequency (no frequency diversity case) has the transmitted signal power of 1 watt. The total power of different diversity branches are taken constant as 1 watt. For 2 diversity branch case, the signals at 2 different branches have 0.5 watt of transmitted signal power.

It is observed from the plot given in Figure 4-12 that EGC performs very close to MRC and SS has the worst performance among these 3 techniques. Because SS uses only 1 branch with the highest SNR value and this branch has a power of 0.5 watt, SS may perform worse than single frequency case with 1 watt of transmitted signal power.

However, the capacity plots have variations and sometimes MRC and EGC may perform worse than single frequency case. This is because of different channel responses for signals at different frequencies. As the frequency separation between

signals changes, the response of the channel changes and the capacity curves oscillate corresponding to the change of channel response.

In addition, the oscillations of the capacity values also occur due to the different distances between transmitter and receiver. For example, at some distance value, if the channel responses for some of the diversity branches come to a minimum point, applying diversity may perform worse than no diversity case but for another distance that may not be the case.

Hence, for a better understanding, the variations of the capacity with respect to different distance values and frequency separations should be examined together. In this section, the plots will be given for two different distances for comparison.

In Figure 4-13, the capacity values are plotted with respect to the frequency separation between 3 diversity branches. For the example in Figure 4-13, three diversity branches have the carrier frequencies of 5 GHz, (5 GHz−Δf) and (5 GHz+Δf) where Δf is the frequency separation between diversity branches. For comparison, capacity value obtained using one carrier frequency (no diversity case) is also given.

In this case, the plot obtained for one frequency (no frequency diversity case) has the transmitted signal power of 1 watt. For 3 diversity branch case, the signals at different branches have 1/3 watt transmitted signal power and the total power is constant.

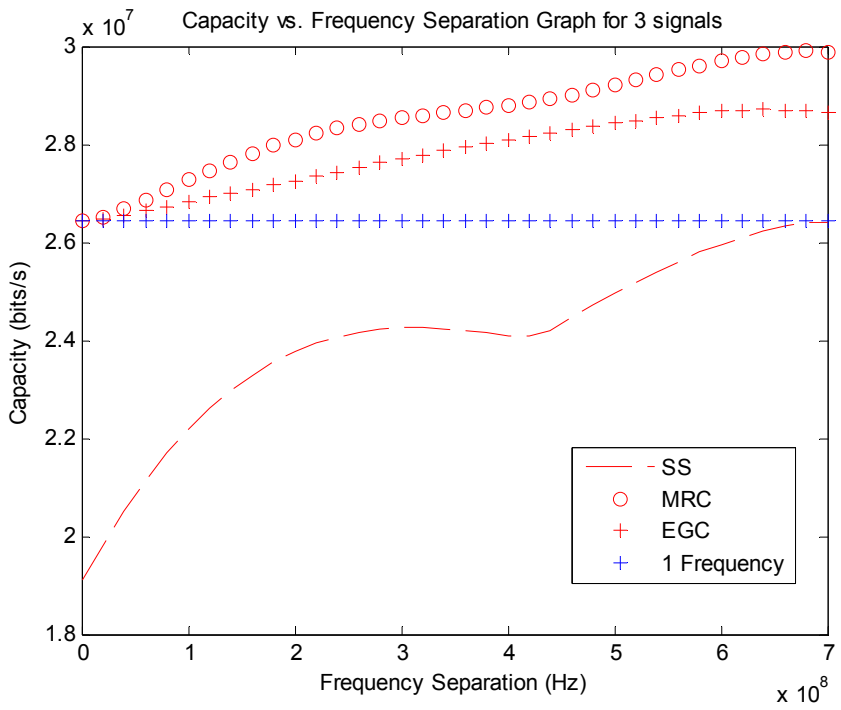

Figure 4-13: Capacity vs frequency separation graph for 3 branches for 9 km

It is observed from the plot given in Figure 4-13 that EGC performs very close to MRC and SS has the worst performance among these 3 techniques. The comments that are made about the effects of distance and frequency separation on system performance for 2 diversity branches case, are also applicable for 3 branches case.

In Figure 4-14, the capacity values are plotted with respect to the frequency separation between 5 diversity branches. For the example in Figure 4-14, five diversity branches have the carrier frequencies of 5 GHz, (5 GHz−Δf), (5 GHz+Δf), (5 GHz−2Δf) and (5 GHz+2Δf), where Δf is the frequency separation between diversity branches. For comparison, capacity value obtained using one carrier frequency (no diversity case) is also given.

In this case, the plot obtained for one frequency (no frequency diversity case) has the transmitted signal power of 1 watt. For 5 diversity branch case, the signals at different branches have 0.2 watt transmitted signal power and the total power is constant.

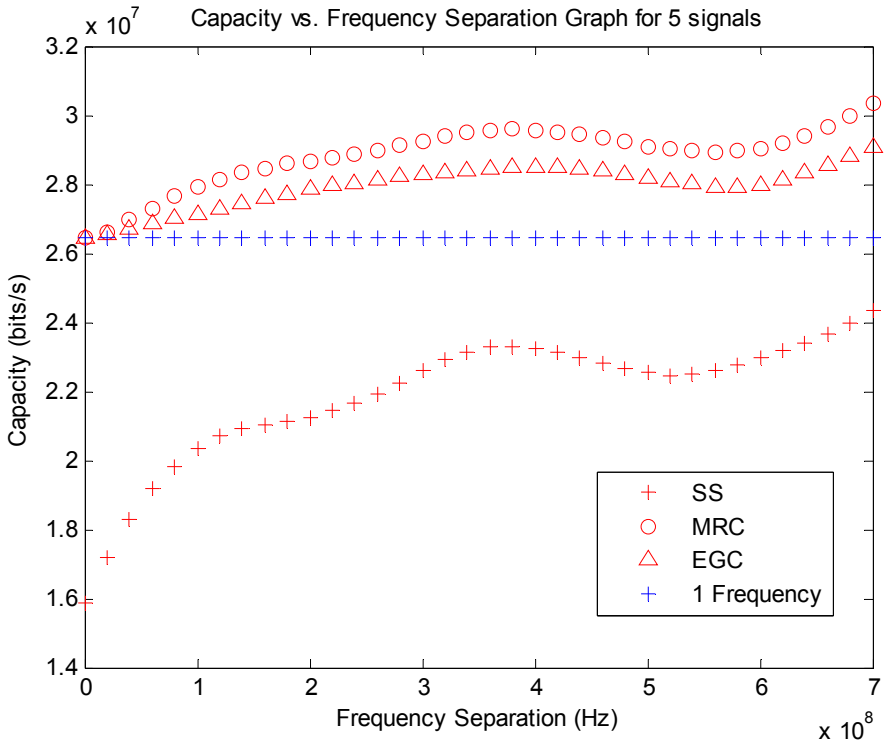

Figure 4-14: Capacity vs frequency separation graph for 5 branches for 9 km

It is observed from the plot given in Figure 4-14 that EGC performs very close to MRC and SS has the worst performance within these 3 techniques. The comments that are made about the effects of distance and frequency separation on system performance for 2 diversity branches case, are also hold for 5 branches case.

In Figure 4-15, the capacity values are plotted with respect to the frequency separation between diversity branches for different number of carriers using MRC and single carrier frequency case (no frequency diversity case).

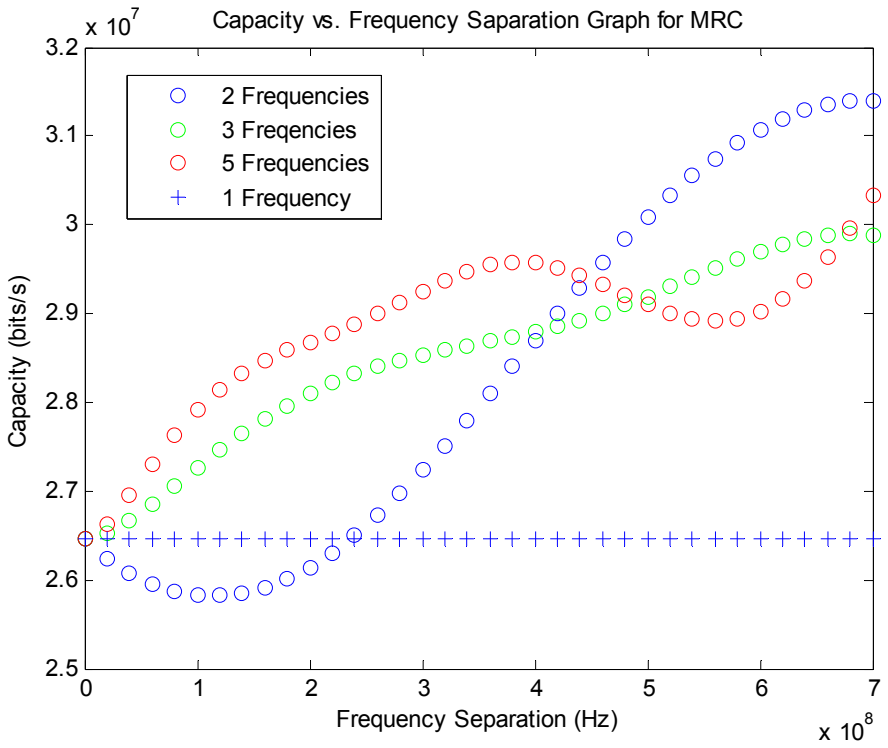

Figure 4-15: Capacity vs frequency separation graph for MRC for different number of branches for 9 km

It is observed that increasing the number of diversity branches may increase the capacity values. However since the channel responses are different for signals at different frequencies, the capacity values oscillate corresponding to the channel response at that frequency. In addition, because the response of the channel changes for different distances, diversity provides different performances for different distances.

In Figure 4-16, the capacity values are plotted with respect to the frequency separation between diversity branches for different number of carriers using EGC and single carrier frequency case (no frequency diversity case).

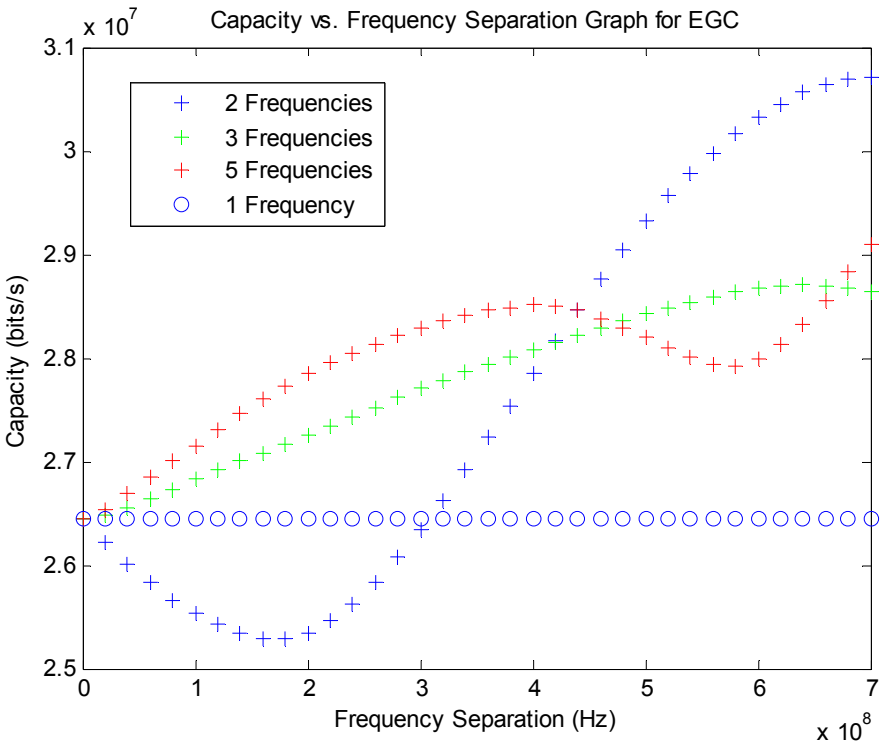

Figure 4-16: Capacity vs frequency separation graph for EGC for different number of branches for 9 km

It is observed that increasing the number of diversity branches may increase the capacity values, however at some other distance diversity may not provide better performance. It is also observed that, all performs the same for no frequency separation case.

In Figure 4-17, the capacity values are plotted with respect to the frequency separation between diversity branches for different number of carriers using SS and single carrier frequency case (no frequency diversity case).

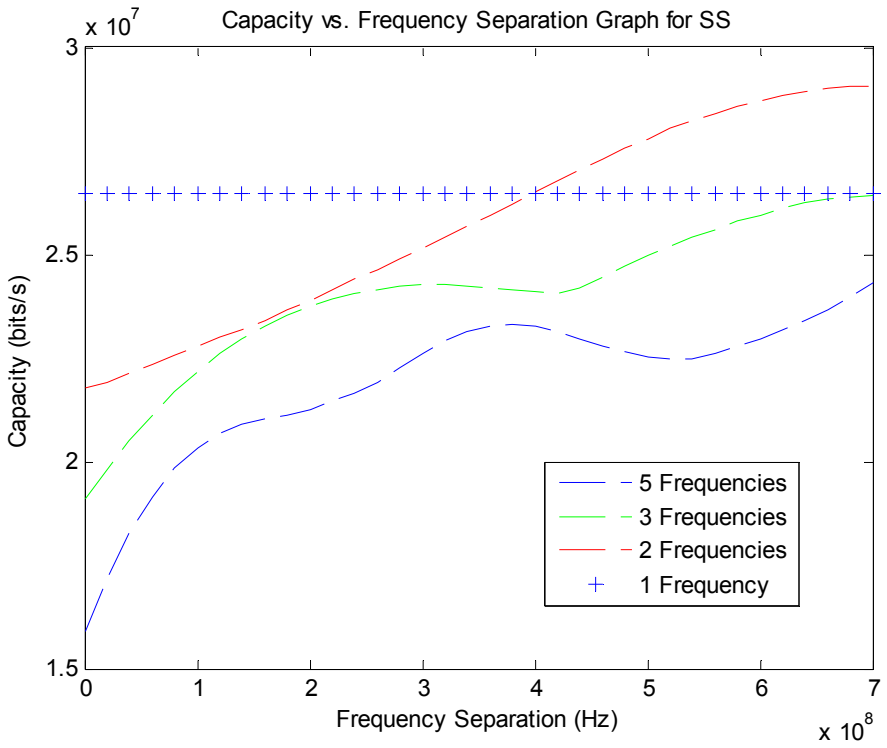

Figure 4-17: Capacity vs frequency separation graph for SS for different number of branches for 9 km

It is observed that increasing the number of diversity branches do not increase the capacity values. Because the total transmitted power remains the same and because SS uses only one branch, it performs worse with increasing number of diversity branches for fixed transmitted power case.

Using the same channel parameters, diversity combining techniques are compared for 12 km distance between transmitter and receiver antennas. The plots in Figure 4-18, Figure 4-19 and Figure 4-20 are obtained.

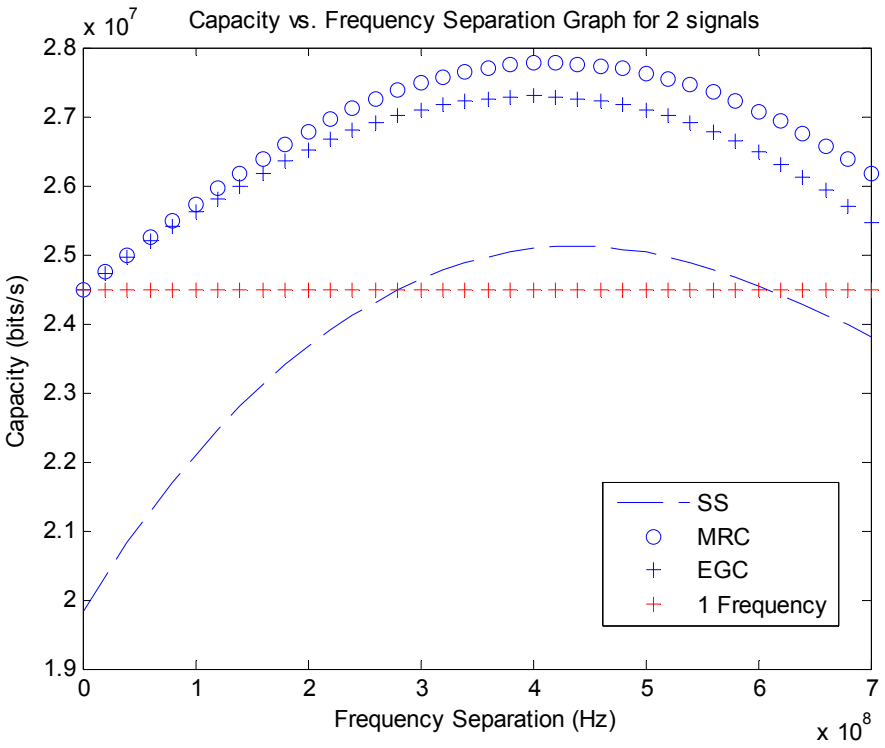

Figure 4-18: Capacity vs frequency separation graph for 2 branches for 12 km

The plot in Figure 4-18 is obtained for 2 branches case. It is observed that EGC performs very close to MRC and SS has the worst performance. When compared with Figure 4-12, it is observed that all combining techniques perform different than the one for 9 km case. MRC and EGC perform better than single frequency case. This occurs because of the fact that the channel response differs for different distances.

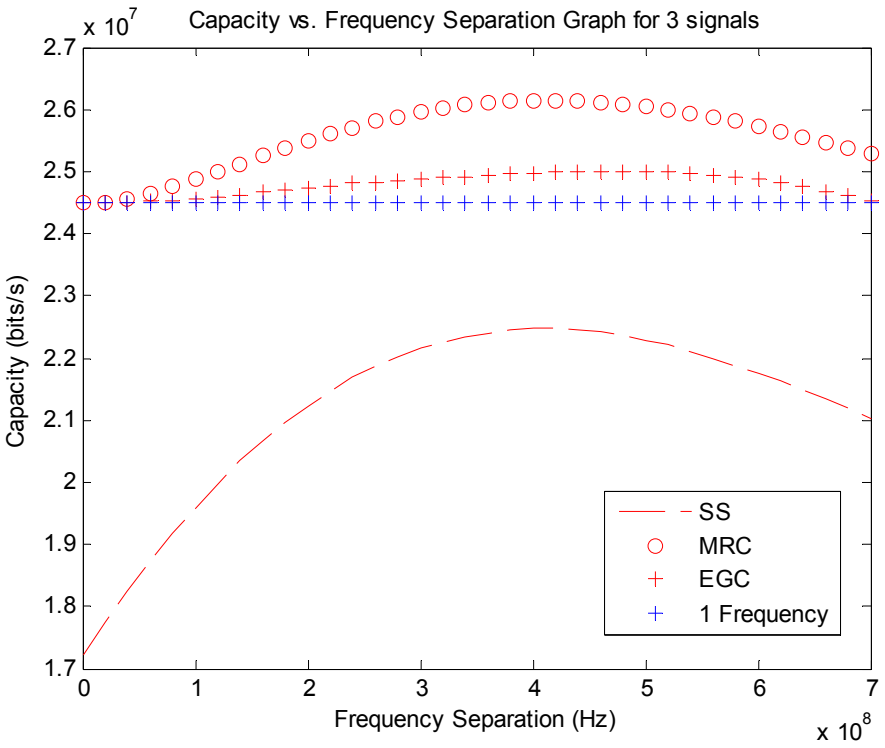

Figure 4-19: Capacity vs frequency separation graph for 3 branches for 12 km

The plot in Figure 4-19 is obtained for 3 branches case for 12 km. When compared with the plot given in Figure 4-13 for 9 km, it is observed that small differences occur in performances of the techniques.

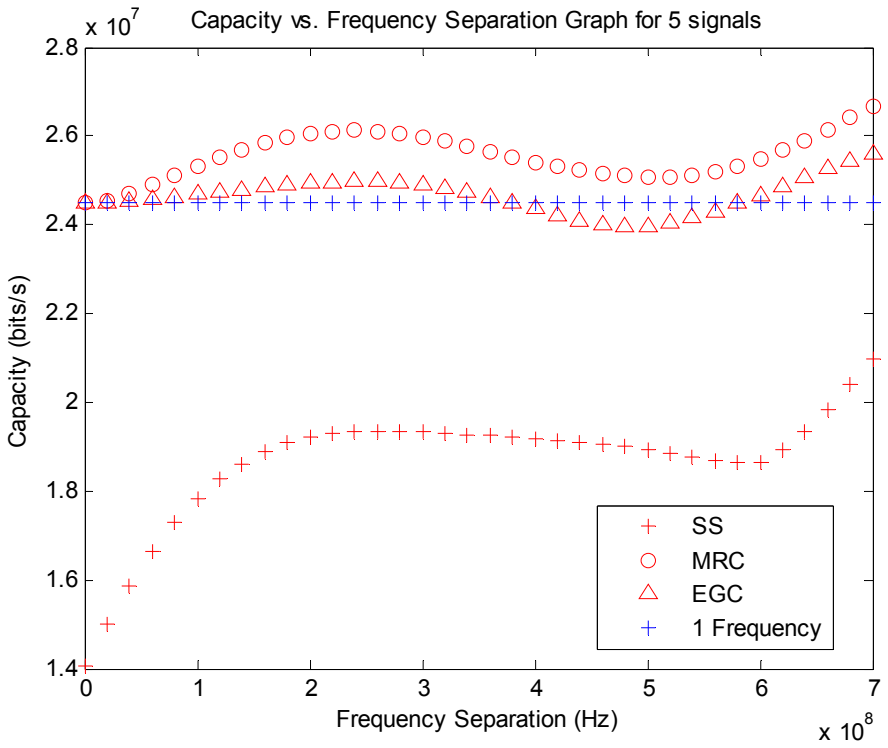

Figure 4-20: Capacity vs frequency separation graph for 5 branches for 12 km

The plot in Figure 4-20 is obtained for 5 branches case for 12 km. when compared with the plot given in Figure 4-14 for 9 km, it is observed that when the frequency separation is increased, MRC and EGC performances get worse, SS performs nearly the same.

When the results are compared for two different distances, it can be concluded that because of the different behavior of channel response for different distances, the performances of the combining techniques become different. For getting a better performance from the frequency diversity system, Channel State Information at the Transmitter (CSIT) should be available at the transmitter side. By this knowledge, transmitter knows where the system gets better performance and arranges the system parameter with respect to the channel state.

Although the two ray channel model does not point to a truly random situation, regarding the coherence bandwidth as suggested by (4-1), we can weakly state that to benefit from the frequency diversity the operation band should be at least in the order of coherence bandwidth. For example, in the scenario considered in this section, from the given Figure 4-4 predicts a coherence bandwidth of around 650 MHz for 9 km. Indeed from Figure 4-12, we see that some gain is possible around such bandwidth.

CHAPTER 5

CUT OFF RATE AND JAMMING EFFECT ON CUT OFF RATE

In this chapter, the cut off rate design tool is reviewed and it is used to predict the performance of an over the sea communication link. Cut off rate analysis may be preferred over the Shannon capacity limit, since it takes the modulation into account.

5.1 CUT OFF RATE AND COMPARISON WITH SHANNON CHANNEL CAPACITY

The algebraic approach and probabilistic approach are the two approaches used for the design of coded modulation. While algebraic approach is concerned with the design of coding and decoding techniques, probabilistic approach is concerned with the analysis of general class of codes [4, 6]. In this section, we will employ the probabilistic approach based on cut off rate.

The cut off rate is one of the important parameters in order to estimate the achievable rate of a digital communication system. Since the use of cut off rate idea by Massey in 1974, the use of cut off rate as an alternative to channel capacity has been common [6, 18, 19].

The most important feature of cut off rate is that it is independent of the specific code employed in the communication system [16].

There are different cut off rate expressions in literature for different modulation techniques and channel properties [17, 18, 19]. In our analysis, we use the cut off rate expression in (5-1) which can be applied to M-ary multi amplitude signals [4, 20].

$$R_o = log_2\left(\frac{q^2}{q + 2\sum_{c=1}^{q-1}(q-c)\exp(-\frac{c^2E_c}{(q-1)^2N_o})}\right)\left(\frac{bits}{dim}\right), \quad (5\text{-}1)$$

where

$R_o : the\ cut\ off\ rate\ \ (bits/\text{dim})$

$q : the\ number\ of\ amplitude\ levels$

$c = \{0, 1, 4, 9, \ldots\ldots (q-1)^2\}$

$E_c : energy\ per\ symbol$

$N_o : the\ noise\ spectral\ density$

Using the cut off rate expression given in (5-1), the cut of rates for different amplitude levels and QAM modulations with different constellations sizes are obtained with respect to changing E_c/N_0. The plots in Figure 5-1 and Figure 5-2 show the related graphs.

For different amplitude levels(q), the cut off rate as a function of SNR is shown in Figure 5-1. The amplitude levels in Figure 5-1 are equally spaced with equal probabilities. The results in Figure 5-2 are obtained by summing the cut off rates for I and Q channels with the assumption that I and Q channels are coded independently. The resultant cut off rate expressions become as follows:

$$R_{o\,(8\,QAM)} = R_{o\,(q=4)} + R_{o\,(q=2)}, \quad (5\text{-}2)$$

$$R_{o\,(16\,QAM)} = R_{o\,(q=4)} + R_{o\,(q=4)}\,, \tag{5-3}$$

$$R_{o\,(32\,QAM)} = R_{o\,(q=8)} + R_{o\,(q=4)}\,, \tag{5-4}$$

$$R_{o\,(64\,QAM)} = R_{o\,(q=8)} + R_{o\,(q=8)}\,, \tag{5-5}$$

where

$R_{o\,(M\,QAM)}$: *the cut off rate for* $M-ary\ QAM$,

$R_{o\,(q=m)}$: *the cut off rate for PAM of level* m.

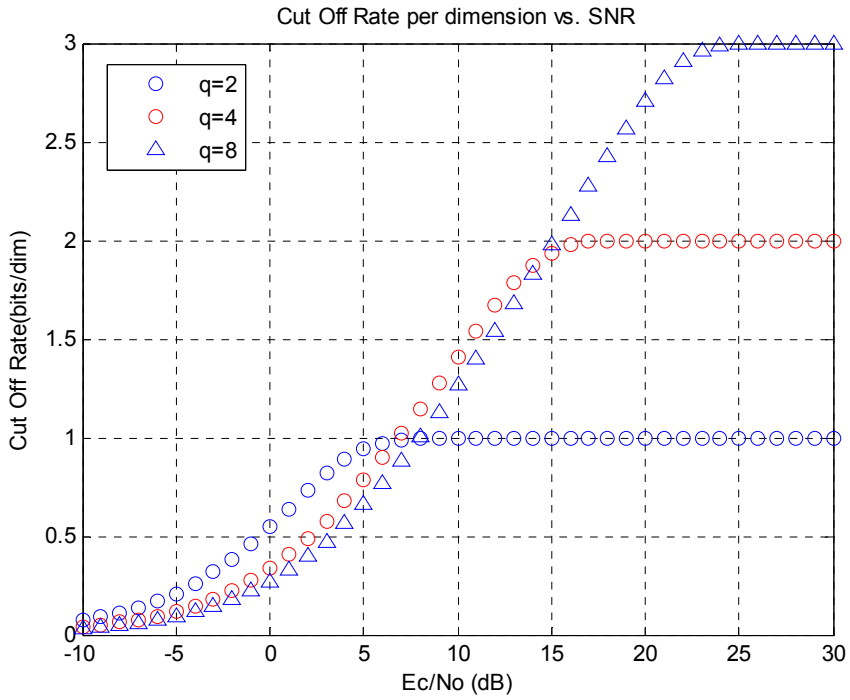

Figure 5-1: Cut off rate graph for several PAM systems

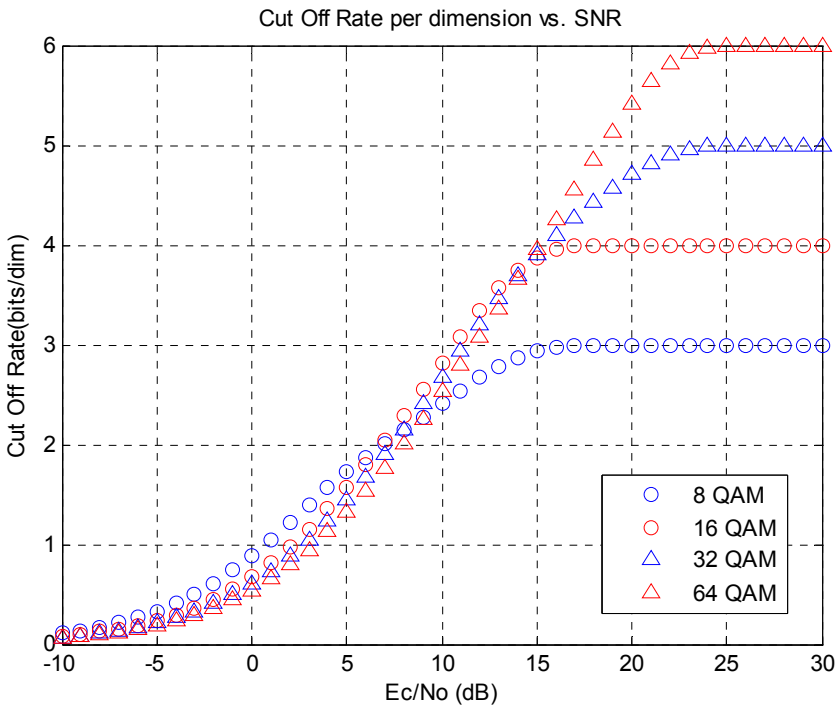

Figure 5-2: Cut off rate graph for QAM

After obtaining cut off rate values for different modulations and constellations, achievable rates obtained using cut off rate can be compared with the capacity values. In this part, the achievable rates are plotted for 2 different distances and they are compared with Shannon capacity values. The plots for the achievable rate and capacity values are obtained with the following specifications:

- The two ray channel model which is defined in Chapter-2 is used as the channel model for both obtaining achievable rates and capacities. In this model, two ships are placed with distances of 5 and 8 km between and the results obtained for 5 km and 8 km distances are plotted at single frequency of 5 GHz. Since typically the grazing angles are very low, polarization is not much important.

- Two omnidirectional half-wave dipole antennas with power gain of 1.64 which are placed on ships as transmitter and receiver antennas are used. The transmitter and receiver antenna heights are chosen as 50 m and 30 m, respectively.
- The standard deviation of surface height σ_h is taken as 1 m, corresponding to the sea state-5 of rough surface.
- Both specular and diffuse components of the reflection coefficients are used. Due to the randomness of the diffuse component of the rough surface reflection coefficient, the experiments of achievable rate and capacity are repeated 1000 times. The achievable rate and capacity values obtained for each experiment are averaged to get the mean capacity.
- The capacity values for 5 km and 8 km are obtained using the Shannon channel capacity expression given in (3-2).
- The cut off rates for QAM modulation of different sizes are obtained using the expressions given in (5-2), (5-3), (5-4) and (5-5). Using the cut off rate values, the achievable rate is obtained by multiplying the cut off rate with available bandwidth with the given expression as follows:

$$R = R_0 \, W \quad \left(\frac{bits}{s}\right), \tag{5-6}$$

where

$R : the\ achievable\ rate,$

$R_0 : the\ cut\ off\ rate,$

$W : the\ channel\ bandwidth.$

- The parameters which are used while obtaining the achievable rate and capacities are summarized in Table 5-1.

Table 5-1: Parameters for plots in Figure 5-3 and Figure 5-4

Parameter		**Value**
Distance	d	5 km & 8 km
Frequency	f	5 GHz
Transmitter antenna height	h_t	50 m
Receiver antenna height	h_r	30 m
Transmitter antenna gain	G_t	1.64
Receiver antenna gain	G_r	1.64
Bandwidth	W	5 MHz
Number of experiments	-	1000

The achievable rate (R) is plotted with respect to the transmitted power in Figure 5-3 and Figure 5-4 for 5 km and 8 km distances respectively using the parameters in Table 5-1 and the channel capacity is also obtained with the same parameters in Table 5-1.

While obtaining the graphs in Figure 5-3 and Figure 5-4, the following expression is used to relate transmitted power (P_t) with E_c/N_0:

$$P_t = E_t\, W\ ,$$

$$E_t = \frac{E_c}{|\alpha|^2}\ ,$$

$$P_t = \frac{E_c}{|\alpha|^2} W\ ,$$

$$P_t = \left(\frac{E_c}{N_0}\right) W \frac{1}{|\alpha|^2}\ \ N_0\ , \tag{5-7}$$

where

$P_t : the\ transmitted\ signal\ power,$

$E_t : the\ transmitted\ signal\ energy,$

$W : the\ bandwidth\ of\ the\ channel,$

α : *the complex attenuation of the channel.*

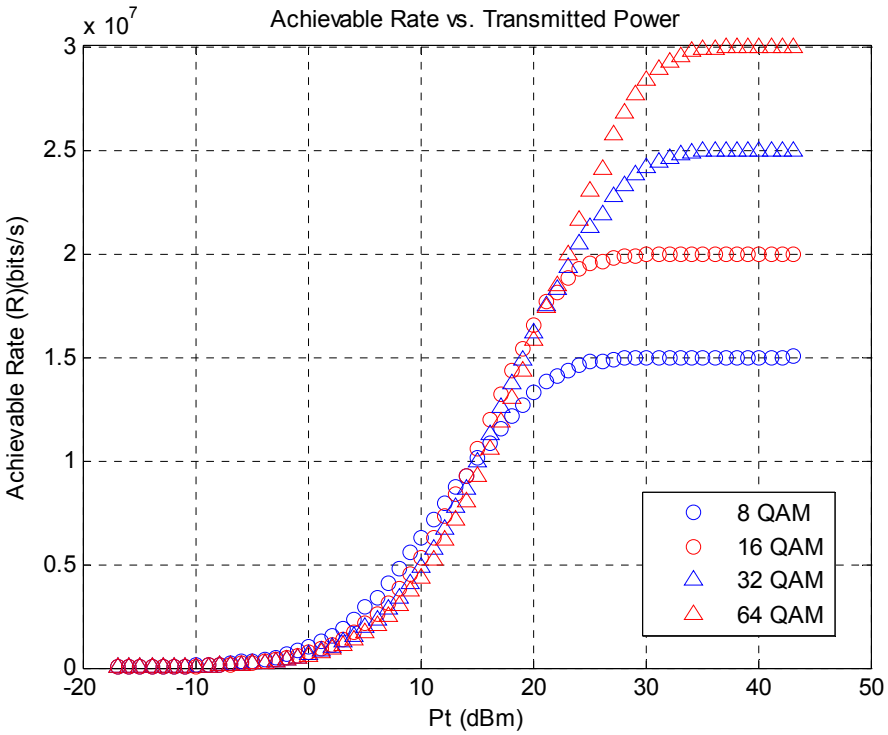

Figure 5-3: Achievable rate vs. transmitted power graph for 5 km

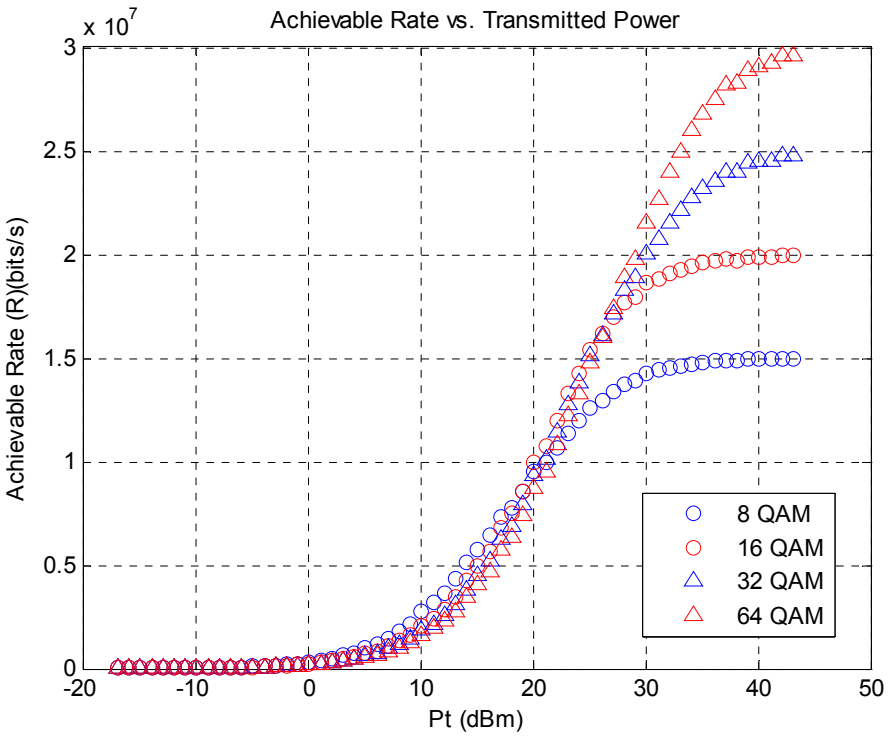

Figure 5-4: Achievable rate and transmitted power graph for 8 km

The channel capacity results are summarized in Table 5-2 for 30 dBm transmitted power for 5 km and 8 km using the parameters in Table 5-1. The achievable rate results plotted in Figure 5-3 and Figure 5-4 are summarized in Table 5-3 for 30 dBm transmitted power case.

Table 5-2: Channel capacity values for 5 km and 8 km

Parameter	**d=5 km**	**d=8 km**
Channel capacity (Mbits/s)	33	27

Table 5-3: Achievable rate values for 5 km and 8 km

Parameter		d=5 km	d=8 km
Achievable rate (Mbits/s)	64 QAM	28	22
	32 QAM	24.5	20
	16 QAM	20	19
	8 QAM	15	14

It is observed form the results in Table 5-2 and Table 5-3 that cut off rate values are below the capacity values and capacity provides a bound for achievable rate values as expected. The achievable rate of the system can be improved by using different modulation techniques. For example, while around a rate of 20 Mbps can be achieved using 32 QAM at 8 km distance between transmitter and receiver antennas, this rate can be increased around 22 Mbps by using 64 QAM modulation. Because, the capacity formula does not take into account the modulation and constellation, it expresses that a rate of around 27 Mbps can be reached.

5.2 THE EFFECTS OF FREQUENCY HOPPING SYSTEM ON CUT OFF RATE

In this section, we consider a frequency hopping system under jamming. In a frequency hopping system, the desired message signal is sent over different carrier frequencies together with coding to provide diversity against fading and jamming effects. A general working scheme of a jamming system is given in Figure 5-5. If the transmitted signal is in the jamming region, it can be jammed. The performance of the system under jamming can be improved using proper coding structures.

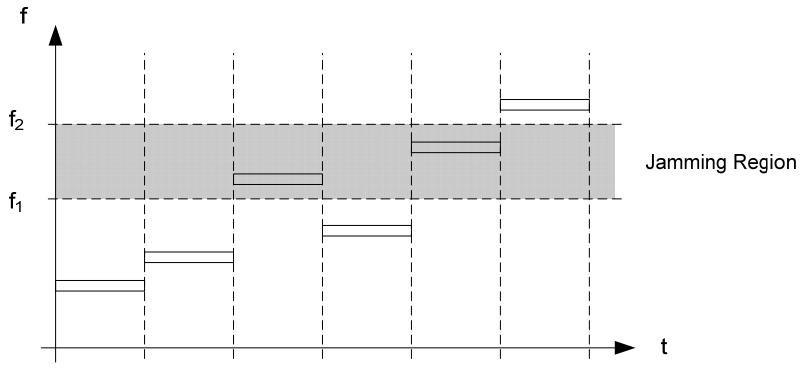

Figure 5-5: Jamming structure

In this work, a block fading model in which each block transmits a piece of information is used in frequency hopping structure. It is assumed that the channel is stationary over each hop and changes independently from hop to hop [6]. The performance of the system is estimated with the cut off rate without using a specific coding structure.

On-off jamming is used for each fading block at different frequencies. Each block is jammed with a given probability. The jammer state vector J which indicates whether the i^{th} block is jammed or not and jammer states at each frequency band are described as follows:

$$J = \{j1, j2 \ldots . jB\}, \tag{5-8}$$

where

$j1, j2 \ldots . jB : jammer\ state\ at\ each\ frequency\ band,$

$$j_i = \begin{cases} 0, & i^{th}\ block\ is\ jammed\ (with\ probability\ \rho) \\ 1, & i^{th}\ block\ is\ not\ jammed\ (with\ probability\ 1-\rho) \end{cases} \tag{5-9}$$

In [6], it is proved that the total cut off rate expression is average of cut off rates of each block not hit by the jammer and the total cut off rate expression is found as follows:

$$R_o(J) = \frac{1}{B}\sum_{i=1}^{B} j_i\, R_i \qquad \left(\frac{bits}{dim}\right), \tag{5-10}$$

where

$R_o(J)$: $the\ cut\ off\ rate\ of\ FH\ system\ of\ B\ blocks,$

R_i : $the\ cut\ off\ rate\ of\ each\ block,$

j_i : $the\ jammer\ state\ at\ i^{th} block$.

The expression in (5-10) is applied to different QAM modulation sizes for different number of blocks and jamming states for investigating the system performance. The plots for the achievable rate values for no jamming case and jamming with jamming probability 0.3 are obtained with the following specifications:

- The two ray channel model which is defined in Chapter-2 is used as the channel model. In this model, two ships are placed with distance of 5 km and the results obtained for 5 km distance are plotted. Since typically the grazing angle is very low, polarization is not much important.
- Two omnidirectional half-wave dipole antennas with power gain of 1.64 which are placed on ships as transmitter and receiver antennas are used. The transmitter and receiver antenna heights are chosen as 50 m and 30 m, respectively.
- The standard deviation of surface height σ_h is taken as 1 m, corresponding to the sea state-5 of rough surface.

- Both specular and diffuse components of the reflection coefficients are used. Due to the randomness of the diffuse component of the rough surface reflection coefficient, the experiments of achievable rate and capacity are repeated 1000 times. The achievable rate and capacity values obtained for each experiment are averaged to get the mean capacity.
- A block fading model is used for frequency hopping structure. 10 blocks are sent at frequencies beginning from 5 GHz to 4.1 GHz with frequency separation of 100 MHz.
- The results are obtained for jamming probability $\rho = 0$ and for jamming probability $\rho = 0.3$ and results are compared.
- The parameters which are used while obtaining the achievable rates are summarized in Table 5-4.

Table 5-4: Parameters of the graph in Figure 5-6 and Figure 5-7

Parameter		**Value**
Distance	d	5 km
Frequency	f	5 GHz
Bandwidth	W	5 MHz
Number of blocks	N	10
Frequency separation between blocks	Δf	100 MHz
Transmitter antenna height	h_t	50 m
Receiver antenna height	h_r	30 m
Transmitter antenna gain	G_t	1.64
Receiver antenna gain	G_r	1.64
Number of experiments	-	1000
Jamming probability	ρ	0 and 0.3

The plots for jamming probability $\rho = 0$ and for jamming probability $\rho = 0.3$ are given in Figure 5-6 and Figure 5-7.

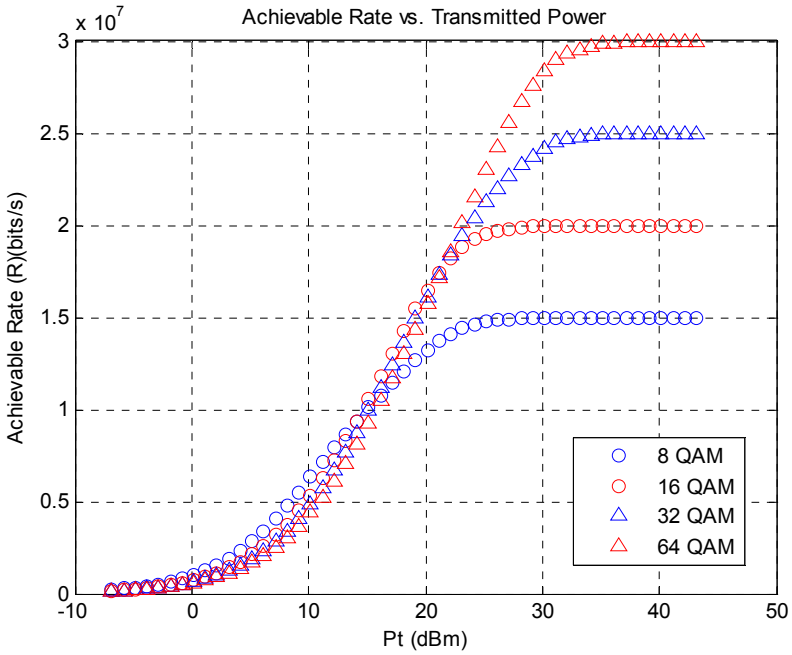

Figure 5-6: Achievable rate graph for no jamming case

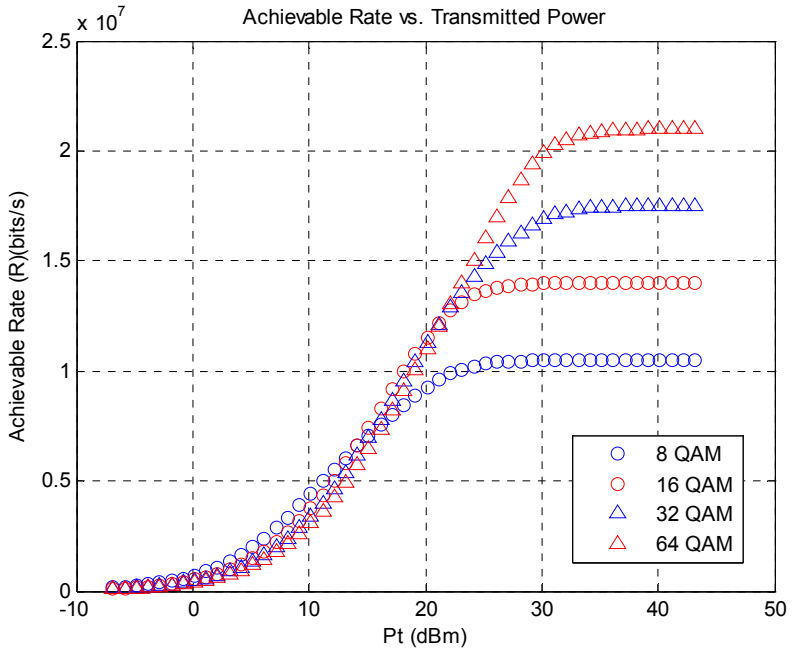

Figure 5-7: Achievable rate graph for jamming probability 0.3

From the plots given in Figure 5-6 and Figure 5-7, it is observed that the rates are decreased due to the effect of jamming. Indeed, for very high SNR operation, the curves saturate at rate $R = (1-\rho)R_N$ where R_N is the achievable rate with no jamming.

5.3 OFDM APPLICATION

In this section, an OFDM system design example is considered. OFDM is a parallel transmission technique, where high-rate serial data stream is split into a set of low-rate sub streams, each of which is modulated on different subcarriers. Because bandwidth of each subcarrier is small compared to the coherence bandwidth of the channel, each subcarrier is assumed to experience flat fading and it is also assumed channel is flat for each block [23].

The achievable rate for OFDM systems are obtained with the following specifications:

- The two ray channel model which is defined in Chapter-2 is used as the channel model. In this model, two ships are placed with distance of 10 km. Since typically the grazing angle is very low, polarization is not much important.
- Two omnidirectional half-wave dipole antennas with power gain of 1.64 which are placed on ships as transmitter and receiver antennas are used. The transmitter and receiver antenna heights are chosen as 50 m and 30 m, respectively.
- The standard deviation of surface height σ_h is taken as 1 m, corresponding to the sea state-5 of rough surface.
- Both specular and diffuse components of the reflection coefficients are used. Due to the randomness of the diffuse component of the rough surface reflection

coefficient, the experiments of achievable rate and capacity are repeated 1000 times. The achievable rate and capacity values obtained for each experiment are averaged to get the mean capacity.

- Block fading model is used and 64 subcarriers are used for each block with different frequencies. Each block with 64 carriers has frequency spacing of 100 MHz and the channel is assumed to be constant for each block.
- In this system, the transmitted signal has 10 blocks. Their frequencies are centered at 100 MHz below 8 GHz in our case.
- Each block has 64 carriers which are modulated by 64-QAM at frequencies centered at block center frequencies. The 48 carriers out of 64 carriers are the data carriers and the others are synchronisation and pilot carriers. Each OFDM symbol has a guard interval of 1/8 of the OFDM symbol time.
- In this expression, the cut off rates of each carrier of different frequency are averaged with respect to the number of fading blocks (N=10 in this case) and number of sub carriers (SUB=64 in this case) in 1 block. The cut of rate of the system is found as follows:

$$R_o = \frac{\sum_{n=1}^{N} \sum_{k=1}^{SUB} R_o\,(n,k)}{N\ SUB}, \tag{5-11}$$

where

R_o : *the total cut off rate,*

$R_o(n,k)$: *the cut off rate for all sub carriers in each block,*

N : *the number of fading blocks,*

SUB : *the number of subcarriers in each block.*

Note that, (5-11) implies that each OFDM subcarrier is coded independently.

- Because of the guard intervals in each OFDM symbol, all the bandwidth is not available. The achievable rate value is obtained by the expression as follows:

$$R = R_o \, SUB \, \frac{1}{t_s}, \tag{5-12}$$

where

SUB : $the\ number\ of\ carriers\ for\ each\ block$,

t_s : $the\ total\ OFDM\ symbol\ time.$

- The parameters which are used while obtaining the cut off rate and the achievable rates are summarized in Table 5-5.

Table 5-5: Parameters of the graph in Figure 5-8 and Figure 5-9

Parameter		**Value**
Modulation	-	OFDM-64 QAM
Distance	d	10 km
Frequency	f	8 GHz
Number of blocks	N	10
Frequency separation between blocks	-	100 MHz
Number of experiments	-	at least 1000
Channel bandwidth	W	20 MHz
Number of carriers for each block	SUB	64
Number of data carriers	$SUBx(3/4)$	48
Frequency separation between the subcarriers	$f_d=W/SUB$	312.5 kHz
OFDM symbol time	$t_{os}=1/f_d$	3.2 microsec.
Guard time	$t_g=t_{os}\ x(1/8)$	0.4 microsec.
Total symbol time	$t_s=t_{os}+t_g$	3.6 microsec

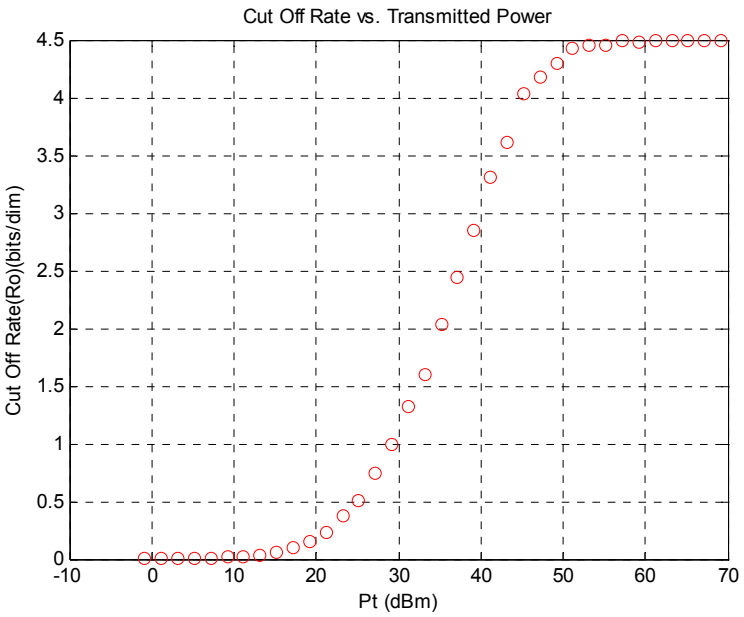

Figure 5-8: Cut off rate graph for system design-1

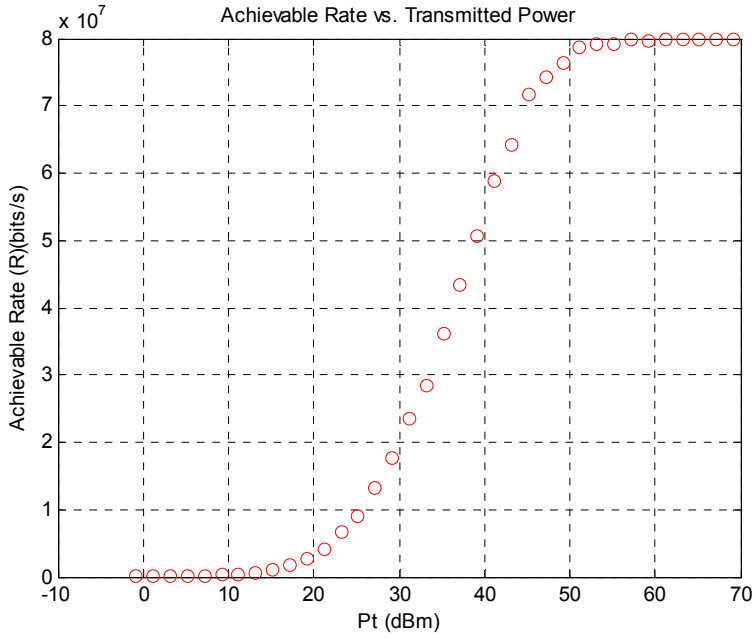

Figure 5-9: Achievable rate graph for system design-1

For these given parameters in Table 5-5, the graphs in Figure 5-8 and Figure 5-9 are obtained. While 64 QAM modulation reaches a cut off rate of 6, in this system due to the pilot and synchronization carriers, we obtained a cut off rate at a lower value.

Another OFDM system may be designed by changing the number of carriers. The same channel model and parameters as OFDM Design-1 are used while obtaining the plots for this system. The parameters that are different than OFDM Design-1 are given in Table 5-6.

Table 5-6: Parameters of the graph in Figure 5-10 and Figure 5-11

Parameter		**Value**
Modulation	-	OFDM-64 QAM
Distance	d	10 km
Frequency	f	8 GHz
Number of blocks	N	10
Frequency separation between blocks	-	100 MHz
Number of experiments	-	at least 1000
Channel bandwidth	W	20 MHz
Number of carriers for each block	SUB	32
Number of data carriers	$SUBx(3/4)$	24
Frequency separation between subcarriers	$f_d=W/SUB$	625 kHz
OFDM symbol time	$t_{os}=1/f_d$	1.6 microsec.
Guard time	$t_g=t_{os}\,x(1/8)$	0.2 microsec.
Total symbol time	$t_s=t_{os}+t_g$	1.8 microsec

The cut off rate and achievable rate results are plotted in Figure 5-10 and Figure 5-11.

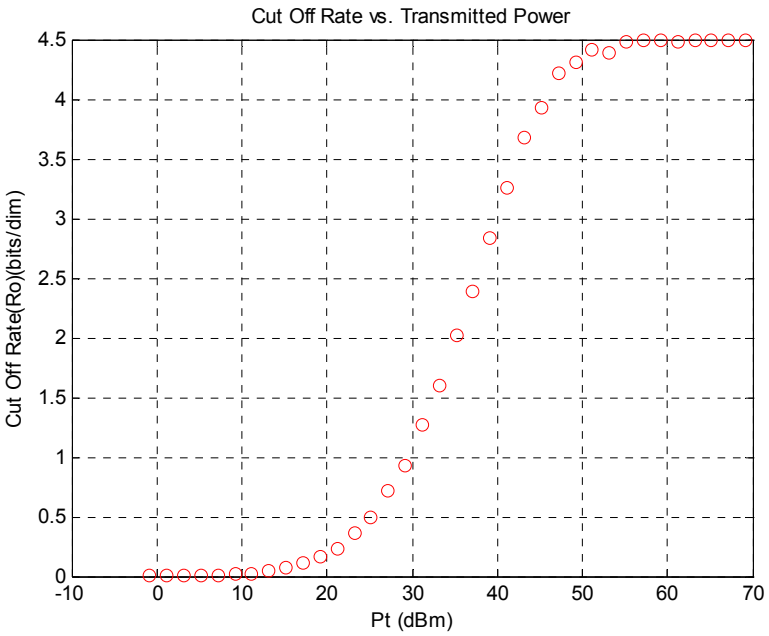

Figure 5-10: Cut off rate graph for system design-2

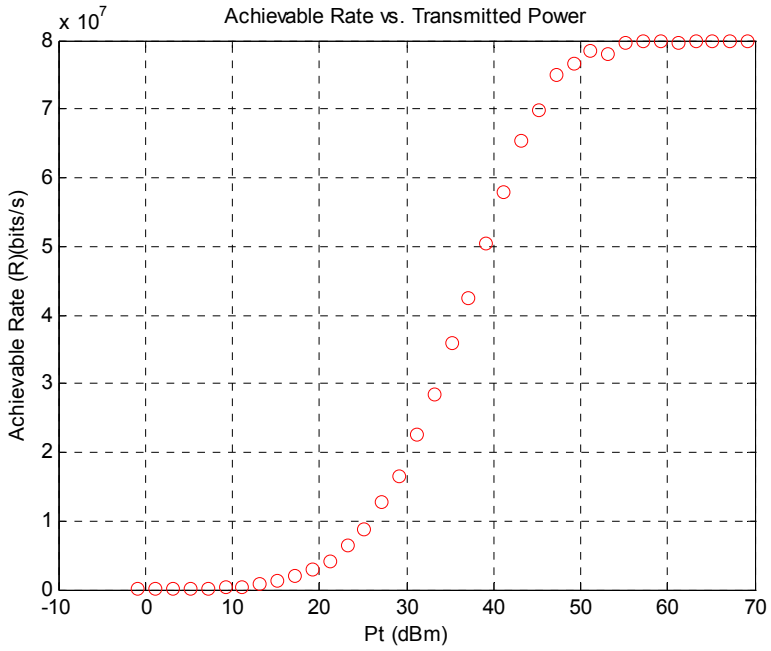

Figure 5-11: Achievable rate graph for system design-2

By comparing Figure 5-8, Figure 5-9, Figure 5-10 and Figure 5-11, we observe that the cut off and achievable rate values are nearly the same with respect to the transmitted power for different number of carriers.

It can be concluded that, the cut off rate and achievable rate values are not affected from the number of carriers.

CHAPTER 6

CONCLUSION

In this work, several tools are developed to aid design of ship to ship high speed communication systems. A two ray channel model is used for microwave communication link. Refraction and reflection coefficients in the model are described and the related formulas are expressed. For the reflected signal, the reflection property of the sea is investigated by considering both the specular and diffuse components of the reflection coefficient.

Using this channel model and related parameters, the path loss and the Shannon channel capacity are obtained. It is observed that significant oscillations occur in the path loss and capacity plots due to the constructive and destructive effects of the reflected signal component. The distance and frequency dependence of path loss and capacity are studied carefully.

Frequency diversity is proposed to be used to combat fading. System performances are analyzed by obtaining the channel capacities using maximal ratio combining, equal gain combining and selection switching methods at the receiver side. It is concluded that, the performance of the system can be increased by using particularly MRC and EGC. It is noted that diversity can be advantageous and disadvantageous depending on the particular distance. Because the channel response changes for different distances and frequency spacing between transmitted signals, the benefit obtained using diversity may change. For example, while MRC and EGC perform better at 12 km than 9 km for 2 branches case, they perform worse at 9 km than 12 km for 5 branches case. These results show that the performance of

these techniques depends on distance and frequency separation. Therefore, CSIT should be used. If the transmitter knows where and how to perform better, it arranges the diversity system in such a manner that the system performance is always improved.

The cut off rate is used as an alternative to Shannon channel capacity. Because Shannon channel capacity does not consider the modulation and constellation, the cut off rate analysis gives more realistic results. Using the two ray channel model and Shannon channel capacity formula, it is seen that a rate around 33 Mbps can be achieved at 5 GHz at a distance of 5 km for 1 watt of transmitted power. The analysis shows that a rate around 24.5 Mbps is obtained using 32 QAM and about 28 Mps rate is obtained using 64 QAM constellations.

Additionally, a frequency hopping system which helps combating both fading and partial band jamming is analyzed. It is observed that this approach can achieve quite satisfactory performance levels.

Finally, as a possible practical solution, a system based on QAM-OFDM is investigated. Using the block fading model and a system using 64 QAM for the subcarriers, transmitted power of about 100 watts can achieve a rate of 80 Mbps over a distance of 10 km.

The following topics can be considered for the future work:

- More parameters for channel model, such as atmospheric effects, more obstacles and antenna motions due to ship's motions, may be examined for more accurate modeling.
- Antenna diversity techniques may be used with or without frequency diversity.
- Networking may be considered in order to improve the overall reliability of the system.

- Use of CSIT must be considered as a means of choosing the best available diversity mode.

REFERENCES

[1] C. Manoj, K. A. Narayanan, B. A. Kota, P. A. Shivaram, A. S. Prasad, R. Ramanathan, *"Investigation of Various ChannelModels for Application of Constant Power Water Filling Algorithm",* Computational Intelligence and Computing Research (ICCIC), 2010 IEEE International Conference on, Pages: 1-7, 2010.

[2] A. Goldsmith*, "Wireless Communications"*, Cambridge University Press, 2005.

[3] T. S. Rappaport, "*Wireless Communications Principles and Practice"*, Prentice Hall PTR, 1996.

[4] John G. Proakis, *"Digital Communications",* Fourth Edition, McGraw-Hill Series,2001.

[5] H. Hourani, *"An overview of Diversity Techniques",* Helsinki University of Technology Lab, S-72.333 Postgraduate Course in Radio Communications 2004/2005.

[6] G. M. Güvensen, Y. Tanık, A. Ö. Yılmaz, *"Cut-off Rate Outage Probability Analysis of Frequency Hopping Mobile Radio under Jamming Conditions"*, Military Communications Conference, 2010-MILCOM 2010, Pages:1684-1689, 2010.

[7] H. R. Anderson, J.P. McGeehan, *"Direct Calculation of Coherence Bandwidth in Urban Microcells Using a Ray-Tracing Propagation Model",* Personal, Indoor and Mobile Radio Communications, 1994, Wireless Networks - Catching the Mobile Future., 5th IEEE International Symposium on, Volume:1, Pages:20-24, 1994.

[8] C. Jakes*," Microwave Mobile Communications",* Wiley- Interscience, 1974.

[9] Q.T. Zhang, S.H. Song, *"Exact Expression for the Coherence Bandwidth of Rayleigh Fading Channels",* Communications, IEEE Transaction on, Volume: 55, Issue: 7, 2007.

[10] M. O. Al-Nuaimi, A. G. Siamarou, *"Coherence Bandwidth Characterisation and Estimation for Indoor Rician Multipath Wireless Channels using Measurements at 62.4 GHz"*, Microwaves, Antennas and Propagation, IEE Proceedings, Volume: 149, Issue: 3, Pages: 181-187, 2002.

[11] A. M. O. Ribeiro, C. S. Castelli, E. M. M. Barrientos, E. Conforti, *" Coherence Bandwidth in a 1.8 GHz Urban Mobile Radio Channel"*, Microwave and Optoelectronics Conference, 2007. IMOC 2007. SBMO/IEEE MTT-S International, Pages: 599-602, 2007.

[12] J. V. O. Goncalves, G. L. Siqueira, *"Delay Spread Calculation from Coherence Bandwidth"*, Microwave and Optoelectronics Conference (IMOC), 2009 SBMO/IEEE MTT-S International, Pages: 253-256, 2009.

[13] F. J. B. Barros, R. D. Vieira, G. L. Siqueira, *"Relationship between Delay Spread and Coherence Bandwidth for UWB Transmission",* Microwave and Optoelectronics, 2005 SBMO/IEEE MTT-S International Conference on, Pages: 415-420, 2005.

[14] R. Liu, Y. Wu, I. Wassell, K. Soga, *"Frequency Diversity Measurements at 2.4 GHz for Wireless Sensor Networks Deployed in Tunnels",* Personal, Indoor and Mobile Radio Communications, 2009 IEEE 20th International Symposium on, Pages: 2990-2994, 2009.

[15] G. Uyar, "*Low Elevation Target Detection and Direction Finding",* Master Thesis, Middle East Technical University, 2012.

[16] D. Rainish, J. M. Perl *"Generalized Cutoff Rate of Time and Frequency Selective Fading Channels",* Communications, IEEE Transactions on, Volume: 37, Issue: 5, Pages: 449-467, 1989.

[17] James L. Massey, *"Coding and Modulation in Digital Communications",* Zurich Seminar, 1974.

[18] S. Misra, A. Swami, L. Tong, *"Cutoff Rate Analysis of the Gauss-Markov Fading Channel with Binary Inputs and Partial CSI at the Receiver",* 2003 Conference on Information Sciences and Systems, The John Hopkins University, 2003.

[19] J. M. Geist, *"Capacity and Cut off Rate for Dense M-ary PSK Constellations",* Military Communications Conference, 1990. MILCOM '90, Conference Record, A New Era. 1990 IEEE, Pages: 768-770, 1990.

[20] Y. Tanık, EE 536 Lecture Notes, Electrical and Electronics Engineering Department-METU, 2012.

[21] T. Griesser, C. A. Balanis, *"Oceanic Low-Angle Monopulse Radar Tracking Errors",* Oceanic Engineering, IEEE Journal of, Volume: 12, Issue: 1, Pages: 289-295, 1987.

[22] C. A. Balanis, *"Antenna Theory",* Third Edition, Wiley, 2005.

[23] R. Prasad, *"OFDM for Wireless Communication Systems",* Artech House Universal Personal Communications Series, 2004.

[24] L. W. Couch, *"Digital and Analog Communication Systems",* Seventh Edition, Prentice Hall, 2007.

[25] World Meteorological Organization, *"Manual on Codes-International Codes",* 1995 Edition.